Surveys in Geophysics (2024) 45:429–458
https://doi.org/10.1007/s10712-023-09814-8

Simultaneous Estimation of P- and S-Wave Velocities by Integrated Inversion of Guided-P and Surface Wave Dispersion Curves

Zhinong Wang[1] · Chengyu Sun[1] · Dunshi Wu[2]

Received: 24 March 2023 / Accepted: 13 October 2023 / Published online: 10 January 2024

Abstract

Compared with surface wave corresponding to the normal mode, which is widely studied, there is less research on guided-P wave corresponding to the leaking mode. Guided-P wave carries the dispersion information that can be used to construct the subsurface velocity structures. In this paper, to simultaneously estimate P-wave velocity (v_P) and S-wave velocity (v_S) structures, an integrated inversion method of guided-P and surface wave dispersion curves is proposed. Through the calculation of Jacobian matrix, the sensitivity of dispersion curves is quantitatively analyzed. It shows that the dispersion curves of guided-P and surface waves are, respectively, sensitive to the v_P and v_S. Synthetic model tests demonstrate the proposed integrated inversion method can estimate the v_P and v_S models accurately and effectively identify low-velocity interlayers. The integrated inversion method is also applied to the field seismic data acquired for oil and gas prospecting. The pseudo-2D v_P, v_S and Poisson's ratio inversion results are of significance for near-surface geological interpretation. The comparison with the result of first-arrival traveltime tomography further demonstrates the accuracy and practicality of the proposed integrated inversion method. Not only in the field of exploration seismic, the guided-P wave dispersion information can also be extracted from the earthquake seismic, engineering seismic and ambient noise. The proposed inversion method can exploit previously neglected guided-P wave to characterize the subsurface v_P structures, showing broad and promising application prospects. This compensates for the inherent defect that the surface wave dispersion curve is mainly sensitive to the v_S structure.

Keywords Surface wave · Guided-P wave · Dispersion curve inversion · Near surface velocity

✉ Chengyu Sun
suncy@upc.edu.cn

[1] China University of Petroleum (East China), Qingdao 266580, China

[2] Research Institute of Petroleum Exploration and Development-Northwest, PetroChina, Lanzhou 730020, China

Article highlights

- Advances in the theory and application of leaking mode and guided-P wave are reviewed. The high sensitivity of guided-P wave dispersion curves to the v_P structures is proved
- An integrated inversion method of guided-P and surface wave dispersion curves is proposed to simultaneously estimate v_P and v_S structures. This compensates for the inherent defect that the surface wave dispersion curves are mainly sensitive to the v_S structure
- The results of synthetic tests and field data application demonstrate the integrated inversion method can characterize the near-surface v_P and v_S structures, which proves the effectiveness and practicability of the proposed method

1 Introduction

Seismic survey plays an important role in the investigation of lithospheric structures and shallow surface (Dorman and Ewing 1962; Aki and Richards 1980). In the past decades, due to the efficient, cost-effective and noninvasive features of the surface wave analysis method, it has been rapidly developed and widely used in many fields (Foti et al. 2018). Although the widely varying investigation scales are various, the applications of the surface wave analysis method are based on the dispersion characteristic of surface wave, which means that different frequency components correspond to different phase velocities (Socco et al. 2010).

Rayleigh wave is a common type of surface waves that propagate along the earth-air interface. It is formed by the interference and superposition of multiple reflections of P and S waves and account for most of the seismic wavefield energy (Rayleigh 1885). Compared with other types of waves, Rayleigh wave is characterized by lower velocity and frequency. By transforming the Rayleigh wave from the time–space domain to the frequency-phase velocity domain, the dispersion images can be obtained (McMechan and Yedlin 1981). The dispersion curves are determined by extracting the trend of dispersion energy peak in the dispersion images (Dai et al. 2021). In a layered earth model, the dispersion equation whose solutions determine the Rayleigh-wave dispersion curve is a nonlinear and implicit function form of the P-wave velocity (v_P), the S-wave velocity (v_S), the mass density (ρ) and the layer thickness (h) (Xia et al. 1999). Sensitivity analysis demonstrates the Rayleigh wave dispersion curves are most sensitive to the v_S, while its sensitivity to the v_P is very low (Cercato 2007). Therefore, the inversion of Rayleigh wave dispersion curves can only be used to estimate the subsurface v_S structures and cannot obtain the reliable v_P structures (Miller et al. 1999). Determining the v_P structures through the empirical relations may result in large deviations.

At present, the widely applied methods of near-surface velocity modeling mainly include first-arrival traveltime tomography and multichannel analysis of surface waves. The first-arrival wave is a type of seismic waves that start from the seismic source and first arrive at the receivers through the underground media. First-arrival traveltime tomography establishes the subsurface v_P structures through the inversion of the first-arrival traveltime (Zhang and Toksoz 1998). The internal mechanism of the two methods of first-arrival tomography and multichannel analysis of surface waves are different, and usually they can only be used to obtain v_P and v_S, respectively. In order to simultaneously obtain the subsurface v_P and v_S structures, researchers proposed joint inversion methods to comprehensively utilize the information of first arrival and surface waves (Ivanov et al. 2006; Dal Moro and Pipan 2007; Boiero and Socco 2014). However, first-arrival traveltime tomography suffers from inherent limitations associated with velocity-inversion interfaces (the overlying velocity is higher than the velocity of underlying stratum) and low-velocity structures, because most raypaths of first-arrival waves cannot pass through the velocity-inversion interfaces and low-velocity structures. This might corrupt the tomographic solutions, and even result in inaccurate estimation of velocity and interface depth. On the other hand, dispersion curve inversion can effectively identify low- or high-velocity interlayer structures, thereby compensating for the defects of first-arrival traveltime tomography (Wang et al. 2023).

Theoretically, homogeneous horizontal layered subsurface structures can be approximated as waveguide systems (Robertsson et al. 1996). For the closed elastic waveguide structures, the normal modal solutions of the dispersion equation are typically described by real-valued wavenumbers, which means the waves have a constant amplitude during propagation (Aki and Richards 1980; Sun et al. 2021). Surface wave, including Rayleigh and Love waves, correspond to normal modes whose energy is confined in the waveguide structure, i.e., for which the motion decreases with depth in the substratum. Nevertheless, for the semi-open elastic waveguide structures, it is well known the oscillation energy is gradually lost in the form of radiation toward the remote boundary of the open region, thereby reducing the oscillation amplitude (Monticone and Alu 2015). Due to the radiation losses, the semi-open waveguide structures can support the complex-valued modal solutions even when the material is ideally elastic, which corresponds to the leaking modes. The seismic wave that controlled by the leaking modes are called the leaky wave (Gao et al. 2014; Jackson et al. 2019). When the phase velocity is higher than the maximum v_S of the semi-open waveguide structure, the energy of leaky wave radiates or leaks into the half-space (Radovich and De Bremaecker 1974). At this time, the amplitude no longer decays exponentially with depth, which violates the existence condition of Rayleigh wave (Phinney 1961). The energy is radiated into the half-space, causing the leaky wave to attenuate along the interface (Haddon 1984). Leaky wave also possesses the dispersion characteristic as surface wave and attracted extensive attention in many fields, including optics (Smith et al. 1991), acoustics (Ryden and Lowe 2004), ultrasonics (Mazzotti et al. 2013), electromagnetics (Goldstone and Oliner 1959), microwave engineering (Hakoda and Lissenden 2018) and nondestructive testing (Lowe 1995).

In earthquake seismology, the free surface and the crust-mantle boundary constitute a semi-open waveguide system. Leaky wave was first noticed by Somville (1930) while studying earthquakes. The trains of long-period dispersive waveforms arriving shortly after the P wave were observed and termed as the PL phase. However, the early development of the PL phase was fundamentally hindered by the limited understanding of the underlying physical mechanism of leaking mode. From the physics viewpoint, Burg et al. (1951) explained that the multiple reflections with incident angles being less than critical angles result in energy leakage out of the waveguide structures. Actually, because of the radiation losses, it was soon recognized that leaking mode is characterized by the complex-valued wavenumber and have an attenuation constant (Rosenbaum 1960). Oliver and Major (1960) used the leaking mode to explain the commonly observed PL phase. They compared the dispersion of PL phase and Rayleigh wave and pointed that Rayleigh wave and PL phase correspond to the normal and leaking modes, respectively. Oliver (1964) determined the phase velocity dispersion and attenuation of PL phase using the observed seismic data propagating in the crust-mantle waveguide. He revealed the apparent dependence of PL phase dispersion on crust-mantle waveguide structures. Furthermore, the information carried by PL phases can provide additional constraint on the model of crust-mantle structure, which is complementary to other types of surface wave data and seismic reflection and refraction data.

By analyzing the attenuation coefficient of PL phase, the leaking modal solutions were divided into the Σ and Π pseudomodes (Cochran et al. 1970). The Π pseudomode is also termed as guided-P mode and more sensitive to the v_P than v_S of the waveguide structure (Su and Dorman 1965). This is a significant difference from normal mode propagation whose sensitivity to v_S is many times greater than v_P. Compared with the widely applied surface wave dispersion curves controlled by the real-valued normal modal solutions, there are rarely studies and applications on the leaking mode dispersion curves. This is mainly due to the difficult of solving the complex-valued leaking modal solutions (Gilbert 1964; Pilant 1972; Watson 1972).

In near-surface seismic surveys, the shallow subsurface velocity structures can provide information in many applications, such as environmental and groundwater study, geological disaster prevention and geotechnical site investigation (Foti et al. 2011). For reflection seismic exploration, the accurate v_P and v_S models of the near surface have great significance for static estimation and correction, multicomponent seismic data processing, migration imaging and the efficiency and effect of the full-waveform inversion (Mari 1984; Ghanem et al. 2017; Pan et al. 2019; Dal Moro 2020; Bohlen et al. 2021; Yang et al. 2022). The shallow surface is generally covered by loose sediment or weathered bedrock. This causes a strong velocity contrast between the free surface and half-space (Sheriff and Geldart 1995). In this view, the stratum between the free surface and high-velocity half-space can be regarded as a semi-open waveguide system (Cox et al. 1999). A large portion of the energy of the recorded seismic wavefields manifests in the form of surface and guided-P waves. Traditionally, these waves have been regarded as the coherent noise that interferes with the identification of reflected events and should be suppressed as much as possible (Wang et al. 2021a, b). However, this results in a waste of near-surface information carried by them. Figure 1a shows a typical land shot gather including obvious Rayleigh and guided-P waves indicated by the orange and pink frames. It can be seen the dispersion characteristic of the guided-P wave produces obvious shingling phenomenon. As shown in Fig. 1b, the

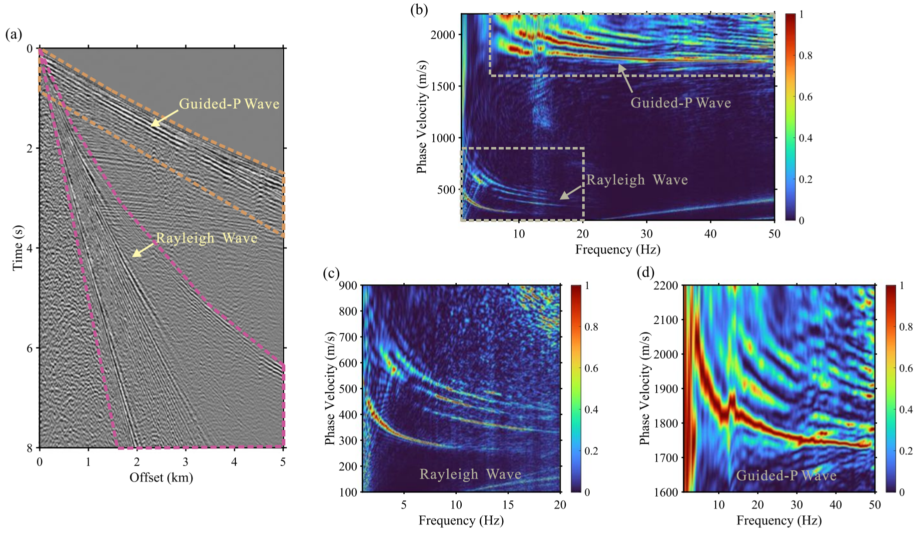

Fig. 1 (**a**) Rayleigh and guided-P waves in the field seismic data; (**b**) Dispersion image of the seismic record in (**a**); (**c**) and (**d**) Rayleigh and guided-P wave dispersion energy corresponding to the seismic records surrounded by the orange and pink frames in (**a**)

corresponding dispersion image is obtained by the phase-shift method (Park et al. 1999). As indicated by the arrows, the dispersion energy of Rayleigh wave is distributed in a low-frequency and low-velocity region. However, the dispersion energy of guided-P wave has a wider frequency band and higher phase velocities. Figure 1c and d shows the dispersion images corresponding to the seismic records surrounded by the orange and pink frames in Fig. 1a. The dispersion energy of Rayleigh and guided-P waves can be observed more clearly.

Roth and Holliger (1999) proposed that, when the shallow subsurface is composed with relatively soft saturated sediments with a high Poisson's ratio, the guided-P wave consists mainly of multi-reflection P wave. Consequently, the dispersion curves of leaking guided-P wave can be closely approximated by the normal acoustic modes. Shtivelman (2004) extracted the dispersion curves of guided-P wave from the field seismic data acquired for shallow offshore surveys and approximated them as normal acoustic modes. By inverting the approximating dispersion curves of normal acoustic modes, the v_P models in the shallow subwater layers were established. Maraschini et al. (2010) presented a new misfit function for multimodal surface wave inversion, which allows higher modes to be used without associating observed dispersion data to specific modes. This avoids mode-misidentification during the inversion. Boiero et al. (2013) applied the method proposed by Maraschini et al. (2010) to the inversion of surface and guided-P wave dispersion data extracted from the land and offshore field seismic data. The inversion results proved that the dispersion information of guided-P wave can be used to construct the near-surface v_P models. Li et al. (2018) presented a wave-equation dispersion inversion method of guided-P waves. The field data application result demonstrated that the proposed method can accurately obtain v_P models at the near surface. Li et al. (2021, 2022) observed and extracted the guided-P waves from the ambient noise and applied their dispersion curves to invert the v_P structures, which demonstrated the potential of guided-P waves in seismology for lithosphere studies. Kennett (2023) introduced the nature of coupling and interacting between multimode surface waves and leaking modes. Fichtner et al. (2023) extracted leaking mode dispersion curves from the distributed fiber-optic sensing data from an airplane landing, which proves the application potential of the leaking mode dispersion curves.

In recent years, with the rapid development of surface wave analysis method, it has been widely studied and applied for constructing near-surface v_S models. However, compared with surface wave, due to the lack of attention and understanding of the dispersion characteristic of guided-P wave, using guided-P wave dispersion curves to estimate near-surface v_P models is not a common practice at present. In this paper, we propose an integrated inversion method of guided-P and surface wave dispersion curves to simultaneously estimate v_P and v_S models. In the Method section, the calculation method of normal and leaking mode dispersion curves is first introduced. Compared with surface wave, guided-P wave dispersion curves are more sensitive to the v_P structures. By constructing an integrated Jacobian matrix including normal and leaking modes, the guided-P and surface wave dispersion curves can be integrally inverted. Then, in the Synthetic Model Test section, the sensitivities of guided-P and surface wave dispersion curves to v_P and v_S are quantitatively analyzed. A velocity increasing model and a low-velocity interlayer model are designed to verify the effectiveness of the integrated inversion method. Besides, the applicability of the method to initial models with different layering strategies is also compared and analyzed. Finally, in the Field Data Application section, the integrated inversion method is applied to the field seismic data acquired for oil and gas prospecting. All 70 set 1D inversion results are interpolated and smoothed to construct the pseudo-2D v_P and v_S profiles. The pseudo-2D velocity profiles are compared with the first-arrival traveltime tomography result and borehole data to demonstrate the accuracy and practicability of the proposed integrated inversion method.

2 Method

2.1 Calculation of Normal and Leaking Mode Dispersion Curves

The accurate and efficient calculation method of dispersion curves is the basis of subsequent inversion. Thomson (1950) first introduced the transfer-matrix method to solve the elastic wave propagation problem in horizontal layered medium. Haskell (1953) developed Thomson's method to deal with the calculation of surface wave dispersion curves. At present, the majority of studies on the calculation methods of dispersion curves mainly focus on the normal mode, including Thomson-Haskell method (Thomson 1950; Haskell 1953), delta matrix method (Dunkin 1965), Schwab-Knopoff method (Knopoff 1964), reflection-transmission matrix method (Kennett 1983) and generalized reflection-transmission coefficients method (Chen 1993). Compared with normal modes, however, there are few studies concerning the calculation and analysis of the leaking modal solutions. The leaking modal solutions are complex numbers, which need to be searched on complex planes (Wu and Chen 2017).

The dispersion curves of both normal and leaking modes are the solutions of the dispersion equation, which is a nonlinear and implicit function of the phase velocity and physical parameters of the layers. First, the problem of elastic wave propagation in a system composed of n plane homogeneous isotropic layers over a half-space is considered. The origin of a two-dimensional Cartesian coordinate system (x, z) is located at the free surface.$v_{P(i)}$, $v_{S(i)}$, $\rho_{(i)}$ and $h_{(i)}$, respectively, represent the v_P, v_S, ρ and h of the ith layer ($i = n + 1$ for the half-space). In the ith layer, the displacement potential functions of P and SV waves can be written as:

$$\begin{cases} \varphi_{(i)} = (A_{(i)}e^{-j\upsilon z} + A'_{(i)}e^{j\upsilon z})e^{j(\omega t-kx)} \\ \psi_{(i)} = (B_{(i)}e^{-j\eta z} + B'_{(i)}e^{j\eta z})e^{j(\omega t-kx)} \end{cases} \quad (1)$$

where $A_{(i)}$ and $A'_{(i)}$ represent the amplitudes of upward and downward P waves, $B_{(i)}$ and $B'_{(i)}$ represent the amplitudes of upward and downward SV waves. k denotes the horizontal wavenumber. υ and η denote the vertical wavenumbers of P and SV waves. ω denotes the angular frequency. $j = \sqrt{-1}$ represents the imaginary unit. The subscript represents the layer number.

According to the continuous conditions of displacement and stress which are satisfied at the interfaces, the recursion relationship between the bottom interface of the ith layer and the top interface of the $(i + 1)$th layer can be established:

$$\left[u_{(i)}, w_{(i)}, \sigma_{zz(i)}, \sigma_{zx(i)}\right]^T = \mathbf{P}_{(i)}\left[u_{(i+1)}, w_{(i+1)}, \sigma_{zz(i+1)}, \sigma_{zx(i+1)}\right]^T \quad (2)$$

where u and w are vertical and horizontal displacements and σ_{zz} and σ_{zx} are vertical and horizontal stresses. The superscript "T" stands for the transpose operator. $P_{(i)}$ represents the transfer matrix of the ith layer. The element expressions of $P_{(i)}$ can be found in the paper of Buchen and Hador (1996).

Considering the surface and radiation conditions at the free surface and half space, the recursion relation between the first layer and half space can be written as:

$$\left[u_{(1)}, w_{(1)}, 0, 0\right]^{\mathrm{T}} = \mathbf{P}_{(1)}\mathbf{P}_{(2)}\ldots\mathbf{P}_{(n)}\left[u_{(\mathrm{n+1})}, w_{(\mathrm{n+1})}, \sigma_{zz(\mathrm{n+1})}, \sigma_{zx(\mathrm{n+1})}\right]^{\mathrm{T}}. \tag{3}$$

After the rearrange of the expression, the dispersion equation or secular function of frequency (f) and phase velocity (c) can be elegantly expressed as the implicit form:

$$s(f,c) = det(UPV) = 0 \tag{4}$$

where U and V represent boundary matrixes according to the top and bottom interlayers. P denotes the transfer matrix, which relates the displacement and stress relationships of the top and bottom interfaces. It is calculated by multiplying the individual transfer matrixes of layers $P_{(1)}P_{(2)} \ldots P_{(n)}$. $det(UPV)$ represents the determinant of these matrix multiplications, which is the value of the secular function for the given frequency, wavenumber and layer parameters (Gilbert and Backus 1966).

In this paper, the fast delta matrix method is adopted to calculate the secular function. It can effectively avoid the problem of precision loss at high frequencies and has high computational efficiency (Buchen and Hador 1996). For normal modes, the solutions of the secular function are found using real values of frequencies and phase velocities (Wang and Herrmann 1980). For leaking modes, assuming the frequency is real, the complex solutions can be found after transforming the problem into the complex velocity plane. The complex-valued secular function is in the form of: $s(f,c) = Re(s)+jIm(s)$. $Re(s)$ and $Im(s)$ represent the real and imaginary parts of the complex-valued secular function $s(f,c)$. The solutions of leaking modes make $Re(s)$ and $Im(s)$ equal to zero at the same time, which correspond to the local minima of the absolute value of the secular function ($|s(f,c)|$) (Znak et al. 2015). Thus, we first find the local minima of $|s(f,c)|$ as the approximate solutions. Then, the approximate solutions are taken as the initial values, and the exact solutions are estimated by the Newton–Raphson method on the basis of the approximate initial values. Finally, a set of dispersion curves are defined by the normal and leaking modal solutions of the secular function.

2.2 Integrated Inversion of Guided-P and Surface Wave Dispersion Curves

The inversion problem of dispersion curves is nonlinear and suffers from the nonuniqueness of the solution (Menke 2012). Including higher-mode information during the inversion can effectively reduce the nonuniqueness, increase the investigation depth, enhance the accuracy of inversion results and stabilize the inversion process. Compared with the global optimization inversion strategy, the local linearized inversion strategy involves very few forward calculations. However, its validity depends on a reliable initial model. In this paper, considering the high computational cost of leaking modes, the least squares linearized inversion strategy is adopted for the integrated inversion method. For the conventional individual inversion of surface wave dispersion curves, usually only the v_S is inverted, and the other layer parameters are all fixed (Xia et al. 1999). By constructing an integrated Jacobian matrix including normal and leaking modes, the sensitivity to v_P can be improved. And the guided-P and surface wave dispersion curves can be integrally inverted to simultaneously estimate the v_P and v_S structures.

Generally, the inversion problem of dispersion curves can be expressed as the following optimization problem:

$$\Phi(\mathbf{m}) = \Phi_d(\mathbf{m}) + \gamma\Phi_m(\mathbf{m}) \rightarrow min \quad (5)$$

where $\Phi(\mathbf{m})$ is the objective function. $\Phi_d(\mathbf{m})$ is the observation data fitting term.

$\Phi_m(\mathbf{m})$ is the model regularization term. $\mathbf{m}$ represents the model parameter vector including v_S and v_P of the layers. γ indicates the regularization parameter (Tikhonov and Arsenin 1977). The objective function can be further rewritten as the following form:

$$\Phi(\mathbf{m}) = \|\mathbf{W}[\mathbf{d} - \mathbf{f}(\mathbf{m})]\|_2^2 + \gamma\left\|\mathbf{L}(\mathbf{m} - \mathbf{m}_{ref})\right\|_2^2 \quad (6)$$

where $\mathbf{f}(\mathbf{m})$ represents the dispersion data calculated by forward modeling. $\mathbf{d}$ denotes the vector of observed dispersion data. $\mathbf{m}_{ref}$ denotes the reference model parameter vector containing a priori information, which can constrain the inversion process. $\mathbf{W}$ denotes the weight matrix composed of the reciprocal of data variance (Cardarelli and Fischanger 2006). $\| * \|_2^2$ represents the square of L2 norm. $\mathbf{L}$ denotes the smoothness matrix formed by the discrete form of Laplace operator (Constable et al. 1987):

$$\mathbf{L} = \begin{bmatrix} 0 & & & & 0 & \\ -1 & 1 & & & & \\ & -1 & 1 & & & \\ & & -1 & \ddots & & \\ & & & \ddots & 1 & \\ & 0 & & & -1 & 1 \end{bmatrix}. \quad (7)$$

Finally, the following linear equation can be used to represent the optimization problem. The updates of model parameters are obtained by iterative calculation:

$$\tilde{\mathbf{A}}\mathbf{m}_{k+1} = \tilde{\mathbf{d}} \quad (8)$$

where $\widetilde{\mathbf{A}}=[\mathbf{W}\boldsymbol{J}(\mathbf{m}_k),\mathbf{L}\sqrt{r}]^T$, $\widetilde{\boldsymbol{d}}=[\boldsymbol{W}\widehat{\boldsymbol{d}}(\boldsymbol{m}),\boldsymbol{L}\boldsymbol{m}_{ref}\sqrt{r}]^T$, $\hat{\mathbf{d}}(\mathbf{m}_k) = \boldsymbol{d}(\mathbf{m}_k) - \mathbf{f}(\mathbf{m}_k) + \mathbf{J}(\mathbf{m}_k)\mathbf{m}_k$. T represents the transpose operation. k indicates the iteration number. And $\mathbf{J}$ represents the Jacobian matrix, which indicates that the phase velocity data as a function of frequency possess different resolving power for determining velocities at different layers (Socco and Strobbia 2004). For the conventional individual inversion method, the elements of the Jacobian matrix $\mathbf{J}_{Indi}$ are the first-order partial derivatives of phase velocity with respect to v_S (Xia et al. 1999):

$$\mathbf{J}_{\mathrm{Indi}} = \partial\ln\mathbf{c}_{\mathrm{S}}/\partial\ln\boldsymbol{v}_{\mathrm{S}} = \begin{bmatrix} \partial\ln c_{\mathrm{S}1}/\partial\ln v_{\mathrm{S}1} & \cdots & \partial\ln c_{\mathrm{S}1}/\partial\ln v_{\mathrm{SM}} \\ \partial\ln c_{\mathrm{S}2}/\partial\ln v_{\mathrm{S}1} & \cdots & \partial\ln c_{\mathrm{S}2}/\partial\ln v_{\mathrm{SM}} \\ \vdots & \ddots & \vdots \\ \partial\ln c_{\mathrm{SN1}}/\partial\ln v_{\mathrm{S}1} & \cdots & \partial\ln c_{\mathrm{SN1}}/\partial\ln v_{\mathrm{SM}} \end{bmatrix}, \quad (9)$$

where ln is the natural logarithm operator and c_S stands for the observed phase velocity of surface waves. M represents the layer number of the model. N1 represents the number of the observed surface-wave dispersion data. By solving the logarithmic versions of the velocity parameters, the stability of inversion can be improved (Vozoff and Jupp 1975).

For the proposed integrated inversion method, the Jacobian matrix J_{Inte} is extended to contain the first-order partial derivatives of surface and guided-P wave phase velocities with respect to v_S and v_P:

$$\begin{bmatrix} \partial \ln c_{S1}/\partial \ln v_{S1} & \cdots & \partial \ln c_{S1}/\partial \ln v_{SM} & \partial \ln c_{S1}/\partial \ln v_{P1} & \cdots & \partial \ln c_{S1}/\partial \ln v_{PM} \\ \partial \ln c_{S2}/\partial \ln v_{S1} & \cdots & \partial \ln c_{S2}/\partial \ln v_{SM} & \partial \ln c_{S2}/\partial \ln v_{P1} & \cdots & \partial \ln c_{S2}/\partial \ln v_{PM} \\ \vdots & \ddots & \vdots & \vdots & \ddots & \vdots \\ \partial \ln c_{SN1}/\partial \ln v_{S1} & \cdots & \partial \ln c_{SN1}/\partial \ln v_{SM} & \partial \ln c_{SN1}/\partial \ln v_{P1} & \cdots & \partial \ln c_{SN1}/\partial \ln v_{PM} \\ \partial \ln c_{G1}/\partial \ln v_{S1} & \cdots & \partial \ln c_{G1}/\partial \ln v_{SM} & \partial \ln c_{G1}/\partial \ln v_{P1} & \cdots & \partial \ln c_{G1}/\partial \ln v_{PM} \\ \partial \ln c_{G2}/\partial \ln v_{S1} & \cdots & \partial \ln c_{G2}/\partial \ln v_{SM} & \partial \ln c_{G2}/\partial \ln v_{P1} & \cdots & \partial \ln c_{G2}/\partial \ln v_{PM} \\ \vdots & \ddots & \vdots & \vdots & \ddots & \vdots \\ \partial \ln c_{GN2}/\partial \ln v_{S1} & \cdots & \partial \ln c_{GN2}/\partial \ln v_{SM} & \partial \ln c_{GN2}/\partial \ln v_{P1} & \cdots & \partial \ln c_{GN2}/\partial \ln v_{PM} \end{bmatrix}, \quad (10)$$

where c_G stands for the observed phase velocity of guided-P wave. N2 represents the number of the observed guided-P wave dispersion data. It should be noted that reliable and accurate calculation of partial derivatives is critical to update the inverted model and significantly affects the convergence of the inversion procedure (Cercato 2007). Here, we adopted the analytical calculation method of phase-velocity partial derivatives based on the combining of the implicit function theorem and the fast delta matrix method (Wu et al. 2019). This ensures the efficiency of partial derivative calculation and the accuracy of inversion. Besides, from the analysis of the sensitivity and Jacobian matrix, the surface and the guided-P waves are mainly sensitive to the v_S and v_P structures, respectively. Therefore, in the process of integrated inversion, the surface wave dispersion information has a higher weight than guided-P waves for the update of the v_S result. On the other hand, the guided-P wave dispersion information has a higher weight than the surface wave for the update of the v_P result.

The misfit function (MF) of the inversion is defined by the relative distance of the observed and estimated dispersion data:

$$\mathrm{MF} = \sqrt{1/N \sum_{j=1}^{N} \left(\frac{c_j^o - c_j^e}{c_j^o} \right)^2} \quad (11)$$

where c_j^e and c_j^o are the estimated and observed dispersion data, N represents the number of the dispersion data. The iteration inversion process will be terminated when any one of the following three stopping criteria is satisfied: 1. MF is smaller than the predefined threshold; 2. MF has converged and is no longer significantly reduced; 3. the iteration number reaches the predefined maximum iteration number.

In Fig. 2a and b, the brief schematic diagrams of the conventional individual inversion and the proposed integrated inversion are presented. The white dotted lines denote the extracted multimode dispersion curves of guided-P and surface waves. It can be seen from the Jacobian matrix of integrated inversion that the dispersion curves of guided-P and surface waves have high sensitivity to v_P and v_S, respectively. By containing the dispersion information of guided-P wave, the sensitivity to v_P can be efficiently improved. Therefore, the v_P and v_S structures can be simultaneously estimated according to the proposed integrated inversion method.

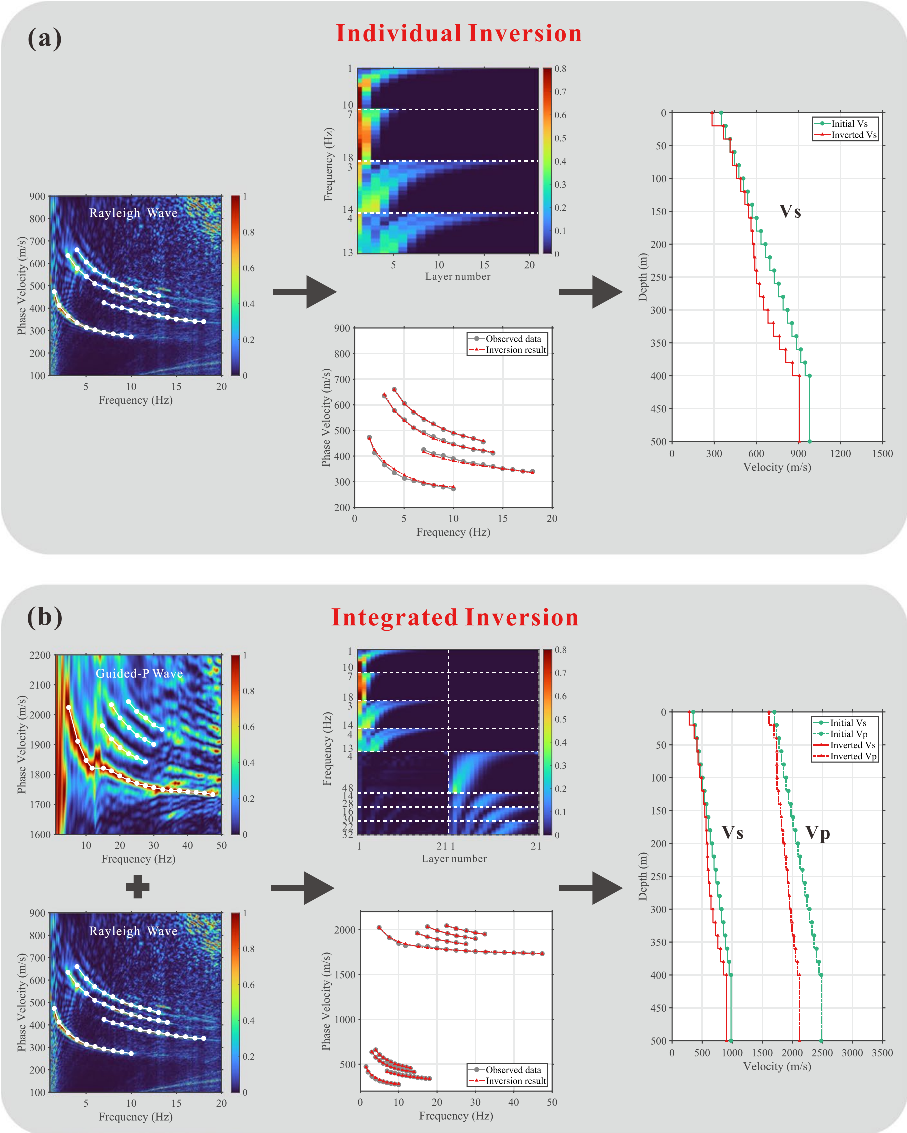

Fig. 2 (**a**) and (**b**) The schematic diagrams of the conventional individual inversion and the proposed integrated inversion

3 Synthetic Model Test

3.1 Model 1

A velocity increasing four-layer model is designed to prove the effectiveness of the integrated inversion method. The parameters of Model 1 are shown in Table 1. According to the computational process described in the previous section, the dispersion curves

Table 1 Structural parameters of Model 1

Layer number	v_P(m/s)	v_S(m/s)	ρ (kg/m^3)	h (m)
1	900	270	1600	5.0
2	1100	330	1600	10.0
3	1300	450	1800	5.0
4	1800	540	2000	∞

containing normal and leaking modes are obtained, as the colored points shown in Fig. 3a. The colors represent the attenuation coefficients calculated according to the relation: $\alpha = -\mathrm{Im}(k) = -\mathrm{Im}(2\pi f / c_{complex})$. In this way, the attenuation extent of each point is also available besides the velocity information. For better distinguishing different modes, the horizontal dashed lines with green and pink colors are also plotted in the figures, representing the maximum and minimum values of v_P and v_S. According to the above analysis, the black points with phase velocities greater than 540 m/s belong to the leaking modes, while the rest belong to the normal modes. Figure 3b demonstrates the locations of the normal and leaking modal solutions on the complex velocity plane. By analyzing the attenuation coefficients and trajectories on complex velocity plane, the leaking modal solutions can be obviously divided into two categories. The leaking modal solutions with significantly smaller attenuation coefficients correspond to the guided-P wave dispersion curves (Cochran et al. 1970). Figure 3c and d shows the separated dispersion curves of surface and guided-P waves. As the frequency increases, the fundamental-mode dispersion curve of guided-P waves tends to approach the minimum v_P of the model. This characteristic is similar to surface wave dispersion curves.

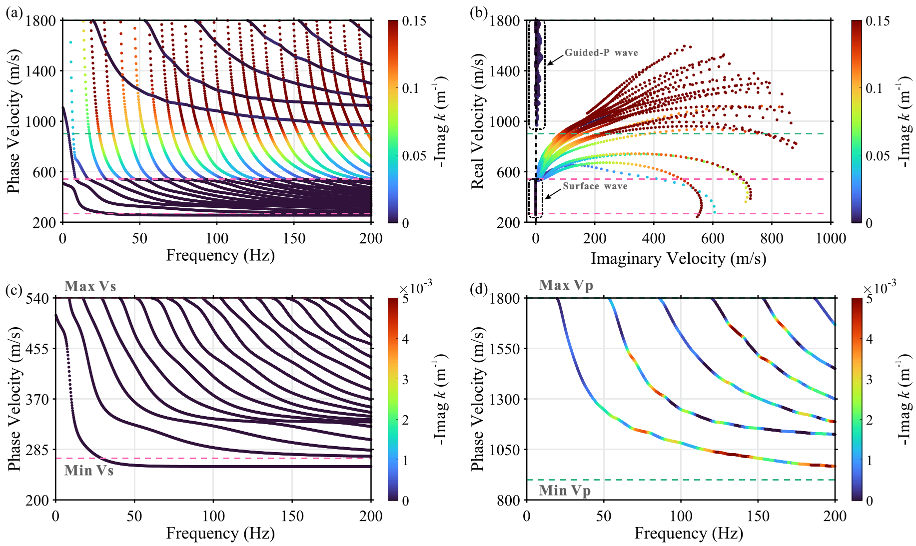

Fig. 3 (**a**) The dispersion curves of Model 1 containing normal and leaking modes; (**b**) The locations of the normal and leaking modal solutions on the complex velocity plane; (**c**) and (**d**) The separated surface and guided-P wave dispersion curves. The horizontal dashed lines with green and pink colors represent the maximum and minimum values of v_P and v_S

Besides, the variation law of the attenuation coefficients of guided-P wave dispersion curves is obviously complicated.

The synthetic seismic record in Fig. 4a is calculated using the finite-difference method (Virieux 1986). A Ricker wavelet is used as source with the dominant frequency of 80 Hz. There are 2000 receivers arranged on the free surface with the spacing interval of 0.25 m to record the seismic wavefields. The recording time is 2.5 s with the sampling interval of 0.05 ms. The size of space grid for finite-difference simulation is 0.25 m × 0.25 m. In order to better distinguish the dispersion energy, we decompose the seismic record into two velocity ranges by FK filtering ($c < 540$ m/s; $c > 900$ m/s), as shown in Fig. 4c and e. The corresponding dispersion images in Fig. 4b, d and f are obtained by phase-shift method. In Fig. 4d and f, the dispersion energy of surface and guided-P waves is in good agreement with the calculated dispersion curves. This demonstrates the accuracy of the calculated dispersion curves.

In order to more intuitively analyze the sensitivity of v_S to surface and guided-P wave dispersion curves, we firstly increase the v_S of the second and third layers of the model by

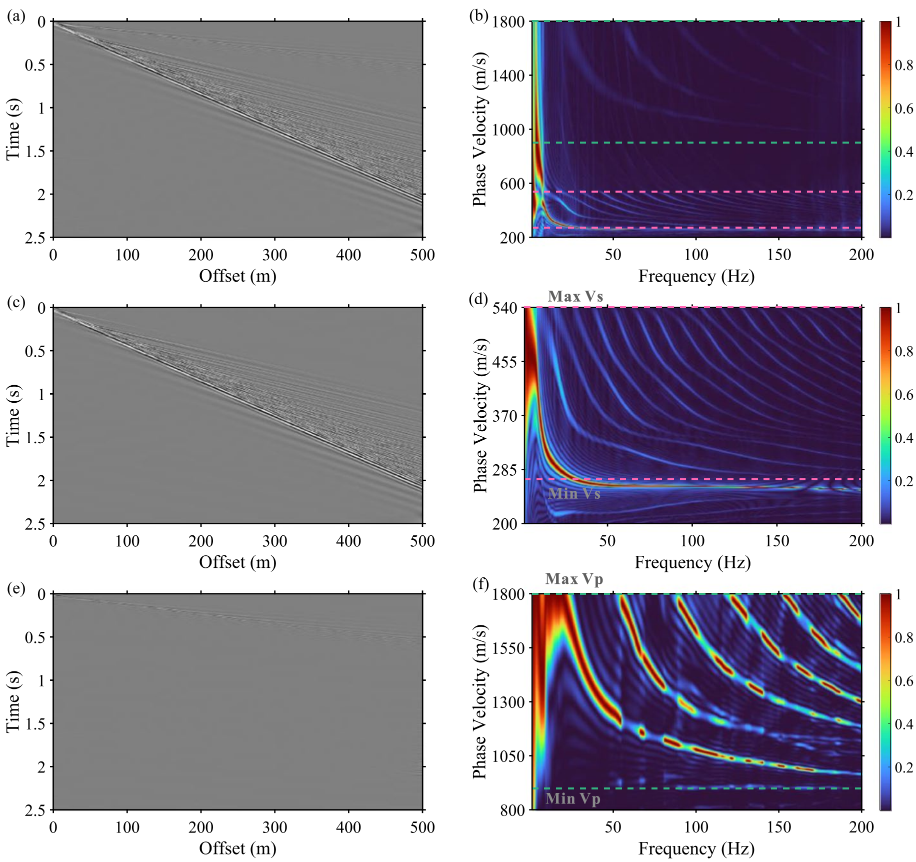

Fig. 4 (**a**), (**c**) and (**e**) The synthetic seismic record of Model 1 and FK filtering results with two velocity ranges ($c < 540$ m/s; $c > 900$ m/s); (**b**), (**d**) and (**f**) The corresponding dispersion images obtained by phase-shift method. The horizontal dashed lines with green and pink colors represent the maximum and minimum values of v_P and v_S

10%, while other parameters of the model remain unchanged. The velocities of the first and last layers are not modified, in order not to change the velocity distribution ranges of the dispersion curves so as to make the comparison with the original dispersion curves more convenient. The dispersion curves after changing the v_S are indicated by the red dots in Fig. 5. The change of the v_S obviously has a much greater influence on the surface wave dispersion curves than that of the guided-P wave dispersion curves. Similarly, we increase the v_P of the second and third layers of the model by 10% and keep other parameters unchanged. The dispersion curves after changing the v_P are indicated by the blue dots in Fig. 5. The change of the v_P has a great influence on the guided-P wave dispersion curves. On the other hand, the surface wave dispersion curves after changing v_P almost coincides with the original dispersion curves. This intuitively proves that the guided-P and surface wave dispersion curves have higher sensitivities to v_P and v_S, respectively.

In order to demonstrate the ability of guided-P wave to constrain the v_P structures, there are three inversion methods considered for comparison. The conventional individual inversion method refers to the inversion of v_S using surface wave. The conventional simultaneous inversion method refers to the inversion of v_S and v_P using surface wave. The proposed integrated inversion method refers to the inversion of v_S and v_P using surface and guided-P waves. Figure 6 shows the results of conventional individual and simultaneous inversion methods using the fundamental and first-high mode dispersion curves of surface wave. The frequency range is from 5 to 100 Hz. In Fig. 6b and c, there are two Jacobian matrixes constructed for conventional individual inversion of v_S and conventional simultaneous inversion of v_S and v_P. Assuming that a priori information can provide accurate stratigraphic stratification, the stratification of the initial model is consistent with the true model. The layer velocities of the initial model are incremental as the green lines shown in Fig. 6d. The Jacobian matrix of individual inversion contains the partial derivatives of surface wave phase velocities with respect to v_S. On the other hand, the Jacobian matrix of simultaneous inversion contains the partial derivatives of surface wave phase velocities with respect to v_S and v_P. The horizontal axis of the Jacobian matrix represents the number of model layers, and the vertical axis represents the frequency of the dispersion data. The white dashed lines separate the regions of v_S, v_P and different modes. As shown in Fig. 6c, due to the low sensitivity of the surface wave dispersion curves to the v_P, its partial derivative value to the v_P is also small. The fitting of the surface wave dispersion curves of the two inversion strategies is presented in Fig. 6a. The dispersion curves obtained by the two inversion strategies can well fit the observed dispersion data.

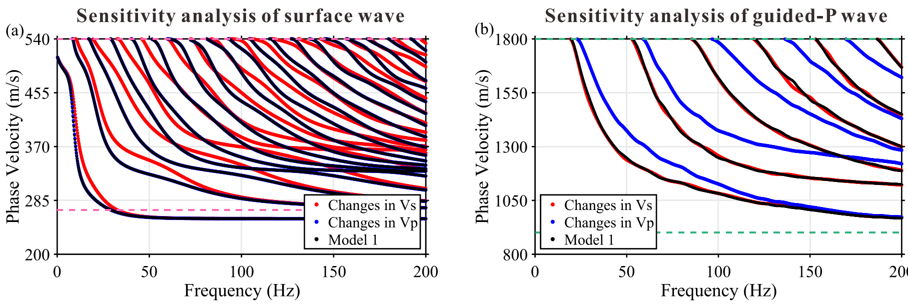

Fig. 5 (**a**) Influence of changing v_S and v_P on the surface wave dispersion curves; (**b**) Influence of changing v_S and v_P on the guided-P wave dispersion curves. The horizontal dashed lines with green and pink colors represent the maximum and minimum values of v_P and v_S

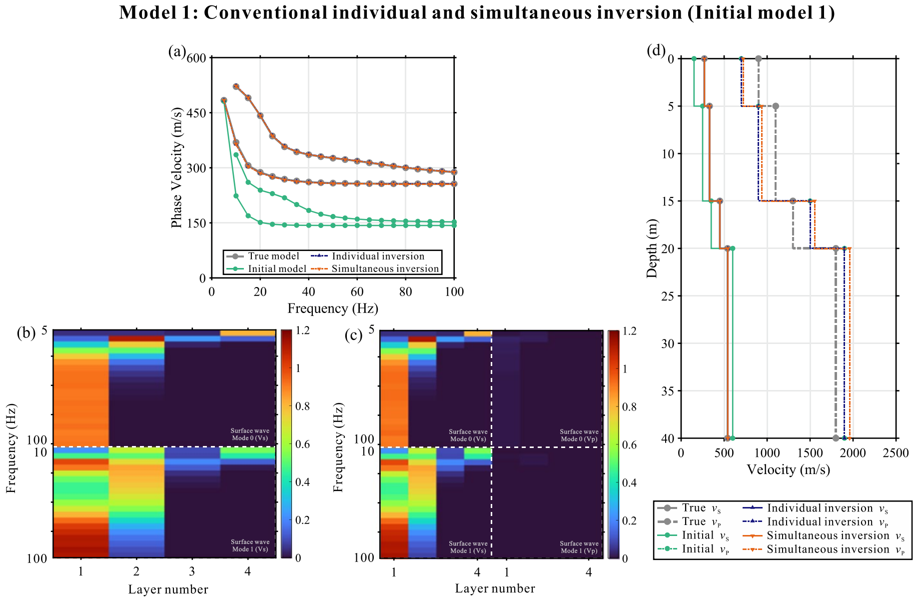

Fig. 6 (**a**) The fitting of the individual and simultaneous inversion results with the observed surface wave dispersion data; (**b**) and (**c**) The Jacobian matrixes of the individual and simultaneous inversion methods; (**d**) The v_S and v_P inversion results of the individual and simultaneous inversion methods

The inversion results are shown in Fig. 6d. The two inversion strategies can both estimate the v_S model accurately. For the individual inversion strategy, the v_P model is fixed during the inversion process. Therefore, its inversion result of v_P coincide with the initial v_P model. For the conventional simultaneous inversion strategy, even if the partial derivative of the surface wave phase velocity to the v_P is included in the Jacobian matrix, the v_P model still cannot be estimated accurately and has a large deviation from the true model. Therefore, it is infeasible to use only the dispersion information of surface wave to invert the v_P structures.

Then, the proposed integrated inversion method is used to estimate the v_S and v_P of Model 1. As demonstrated in Fig. 7a, the surface and guided-P wave dispersion curves can both fit the observed dispersion data well. In Fig. 7b, the corresponding Jacobian matrix shows that, by adding the first and second mode guided-P wave dispersion curves in the inversion procedure, the sensitivity of guided-P wave to v_P is significantly improved and similar to the sensitivity of surface wave to v_S. In Fig. 7c, the v_S and v_P structures can be accurately estimated. This verifies the effectiveness of the proposed integrated inversion method.

When the subsurface stratification is unavailable, the initial model of inversion is usually set to many uniform thin layers. The results of conventional individual and simultaneous inversion strategies are presented in Fig. 8. The two inverted v_S results are almost coincident and their trends are in good agreement with the true model. However, the inverted v_P models are both unsatisfactory. On the other hand, the result of integrated inversion is shown in Fig. 9. To further test the stability of the proposed inversion method, 10% white Gaussian noise is added to the observed dispersion data. It can be seen that the introduction of guided-P wave dispersion information can effectively constrain and improve the inverted v_P model. And the proposed integrated inversion method is robust in the presence of noise.

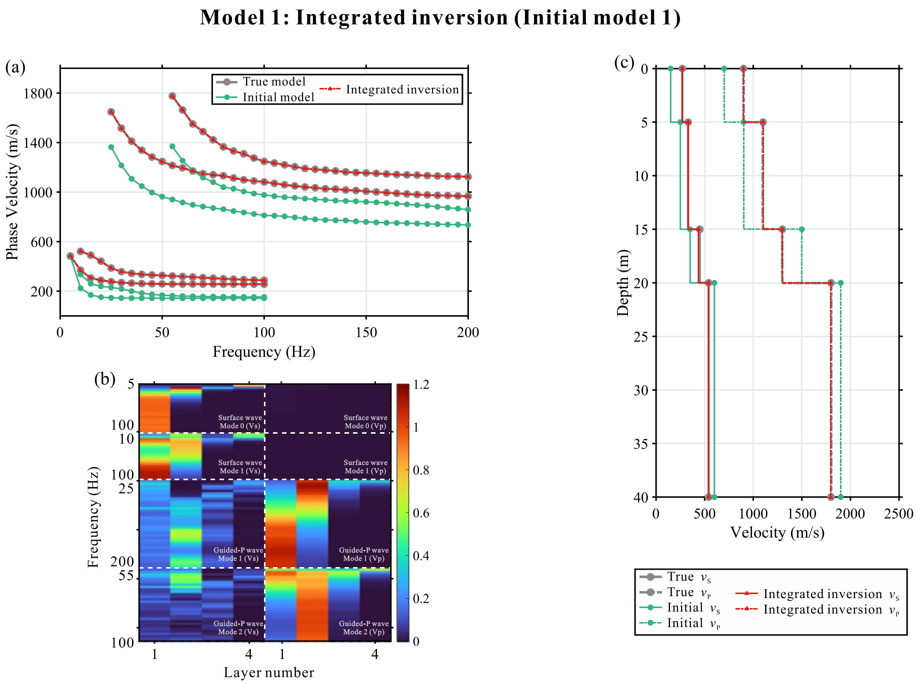

Fig. 7 (**a**) The fitting of the integrated inversion result with the observed surface and guided-P wave dispersion data; (**b**) The Jacobian matrix of the integrated inversion method; (**c**) The v_S and v_P inversion results of the integrated inversion method

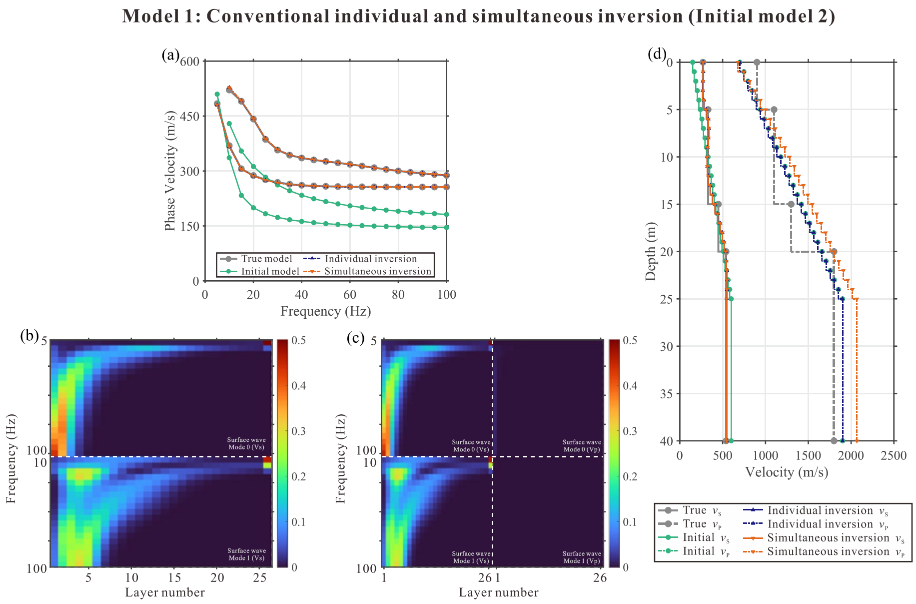

Fig. 8 (**a**) The fitting of the individual and simultaneous inversion results with the observed surface wave dispersion data; (**b**) and (**c**) The Jacobian matrixes of the individual and simultaneous inversion methods; (**d**) The v_S and v_P inversion results of the individual and simultaneous inversion methods

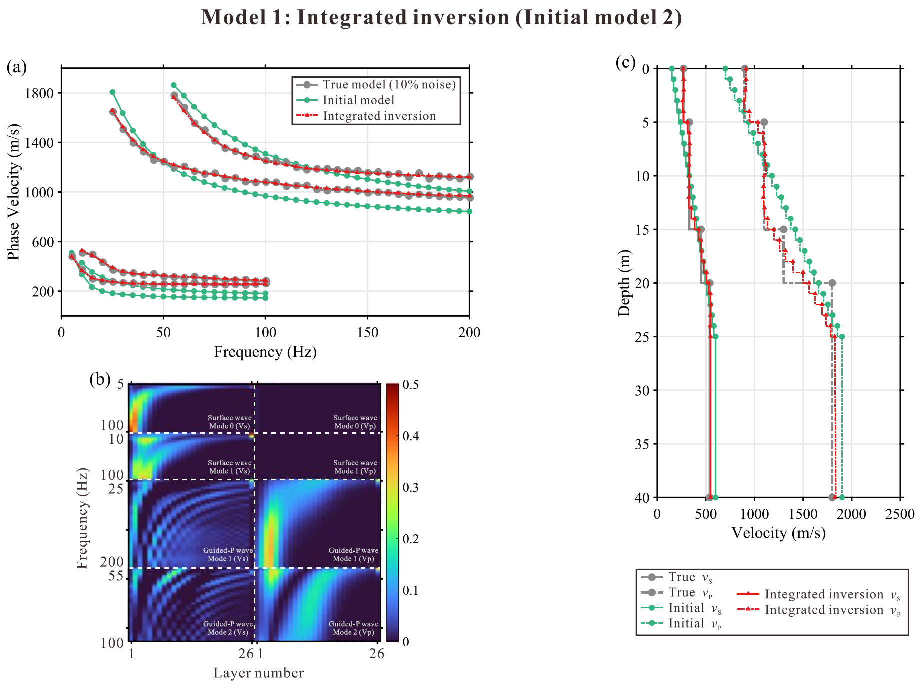

Fig. 9 (**a**) The fitting of the integrated inversion result with the observed surface and guided-P wave dispersion data; (**b**) The Jacobian matrix of the integrated inversion method; (**c**) The v_S and v_P inversion results of the integrated inversion method

3.2 Model 2

A velocity model containing a low-velocity interlayer is designed for further verify the applicability of the proposed method, and the specific parameters are in Table 2. The calculated dispersion curves including normal and leaking modes are shown in Fig. 10a. Figure 10b demonstrates the locations of the normal and leaking modal solutions on the complex velocity plane. The separated dispersion curves of surface and guided-P waves are presented in Fig. 10c and d. Compared with Model 1, the phase velocity and attenuation coefficient of the guided-P wave dispersion curves of Model 2 become more complicated and irregular.

When the stratification of the initial models is consistent with the true models, the comparison of before and after containing the guided-P wave dispersion information is demonstrated in Figs. 11 and 12. For the integrated method, the low-velocity interlayers of v_S

Table 2 Structural parameters of Model 2

Layer number	v_P (m/s)	v_S (m/s)	ρ (kg/m^3)	h (m)
1	900	270	1600	5.0
2	1300	450	1800	10.0
3	1100	330	1600	5.0
4	1800	540	2000	∞

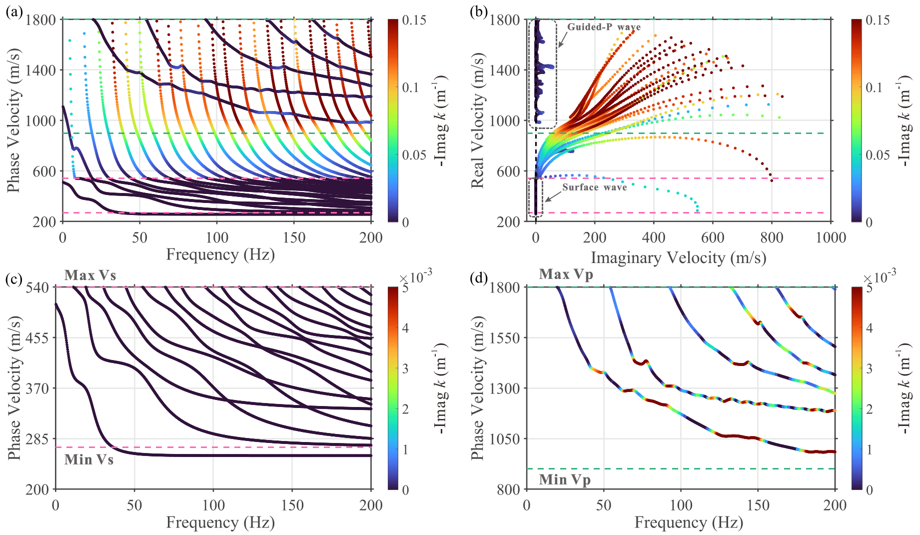

Fig. 10 (**a**) The dispersion curves of Model 2 containing normal and leaking modes; (**b**) The locations of the normal and leaking modal solutions on the complex velocity plane; (**c**) and (**d**) The separated surface and guided-P wave dispersion curves. The horizontal dashed lines with green and pink colors represent the maximum and minimum values of v_P and v_S

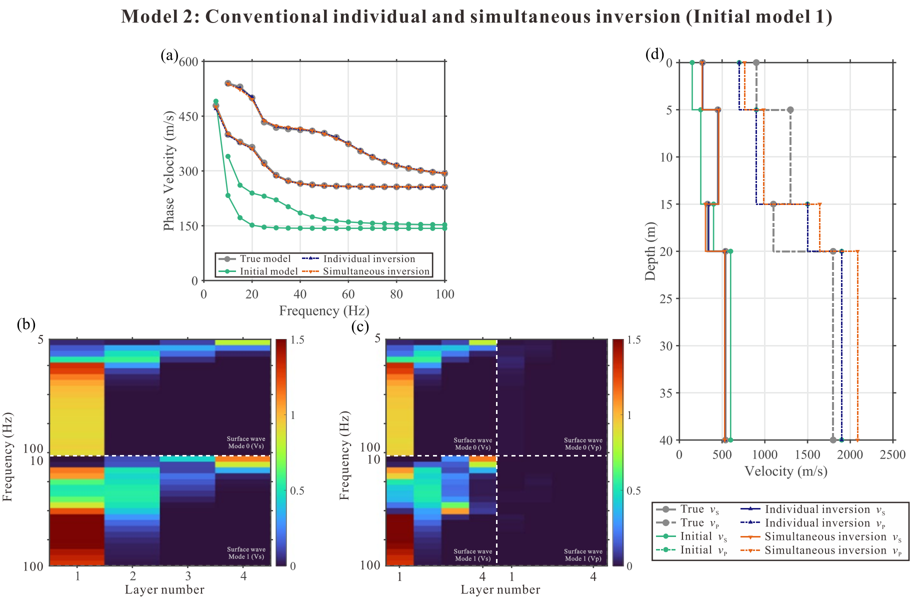

Fig. 11 (**a**) The fitting of the individual and simultaneous inversion results with the observed surface wave dispersion data; (**b**) and (**c**) The Jacobian matrixes of the individual and simultaneous inversion methods; (**d**) The v_S and v_P inversion results of the individual and simultaneous inversion methods

and v_P models can be accurately identified. In the case of setting the initial models with uniform thin layers, although the inverted v_S results cannot clearly distinguish the velocity

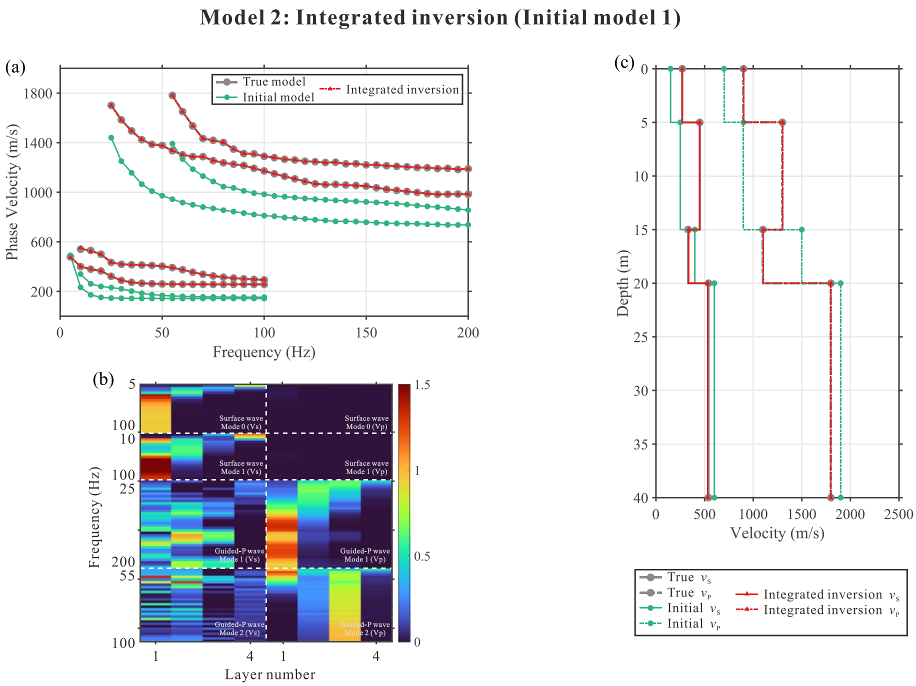

Fig. 12 (**a**) The fitting of the integrated inversion result with the observed surface and guided-P wave dispersion data; (**b**) The Jacobian matrix of the integrated inversion method; (**c**) The v_S and v_P inversion results of the integrated inversion method

interface at the depth of 15 m, they overall trends are still consistent with the true v_S model, as shown in Fig. 13. In Fig. 14, with the addition of 10% white Gaussian noise, the integrally inverted v_S and v_P models can both effectively distinguish the low-velocity layers. Besides, as indicated by the arrow in Fig. 14c, it can be seen that the second mode of the guided-P wave is more sensitive to the v_P of the low-velocity interlayer, which is particularly beneficial to the accurate identification of the low-velocity interlayer.

4 Field Data Application

In Fig. 15, the field shot gathers including obvious Rayleigh and guided-P waves was acquired in Northwest China for oil and gas exploration. The surface sediments within the study area mainly include the silty clay and conglomerate. The bedrock is composed by the marlstone. The recording time of the field seismic data was 7 s, and the sampling interval was 2 ms. The survey line totally contained 35 explosive sources and each source corresponds to 216 receivers. The receivers were linearly distributed along the survey line with the spacing interval of 50 m. The natural frequency of the receivers was 4 Hz. Two dispersion images corresponding to the positive and negative offsets can be obtained from each shot gather. The phase-shift method is used to calculate the dispersion images, and the spatial windows containing 108 seismic traces used for dispersion imaging are indicated by the red frames. Figure 16a–d and e–h is the dispersion images obtained from the negative

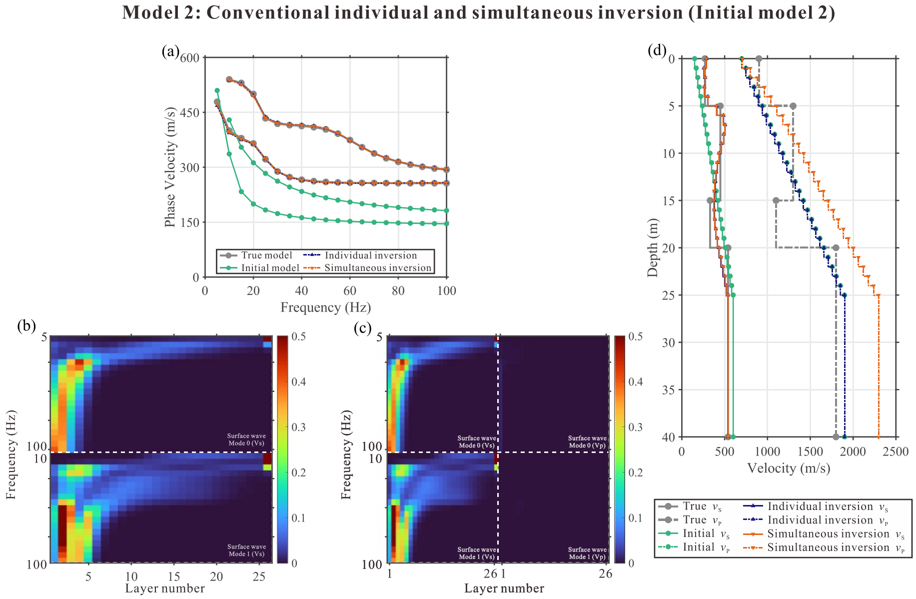

Fig. 13 (**a**) The fitting of the individual and simultaneous inversion results with the observed surface wave dispersion data; (**b**) and (**c**) The Jacobian matrixes of the individual and simultaneous inversion methods; (**d**) The v_S and v_P inversion results of the individual and simultaneous inversion methods

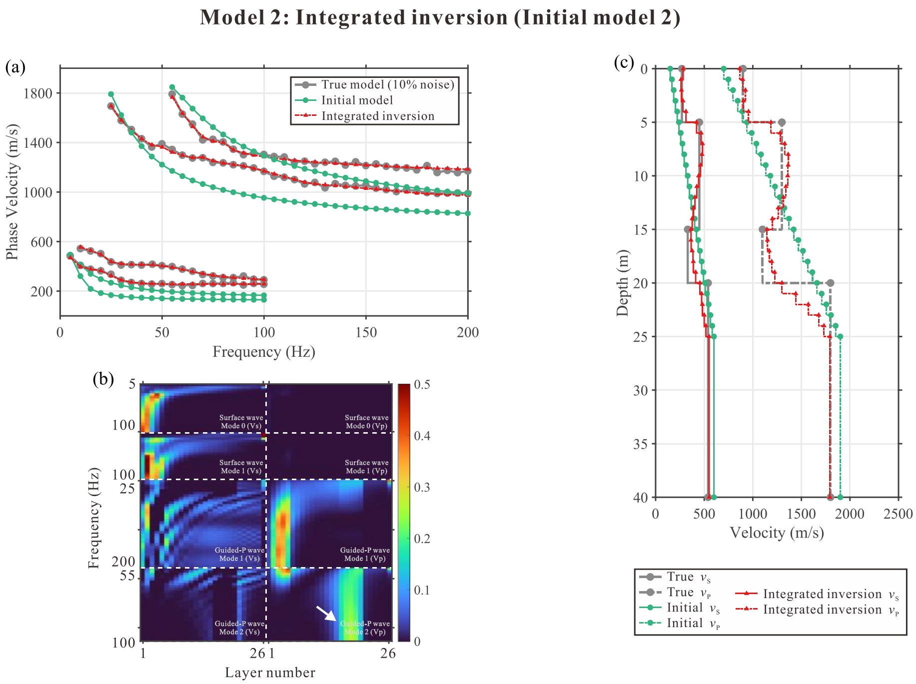

Fig. 14 (**a**) The fitting of the integrated inversion result with the observed surface and guided-P wave dispersion data; (**b**) The Jacobian matrix of the integrated inversion method; (**c**) The v_S and v_P inversion results of the integrated inversion method

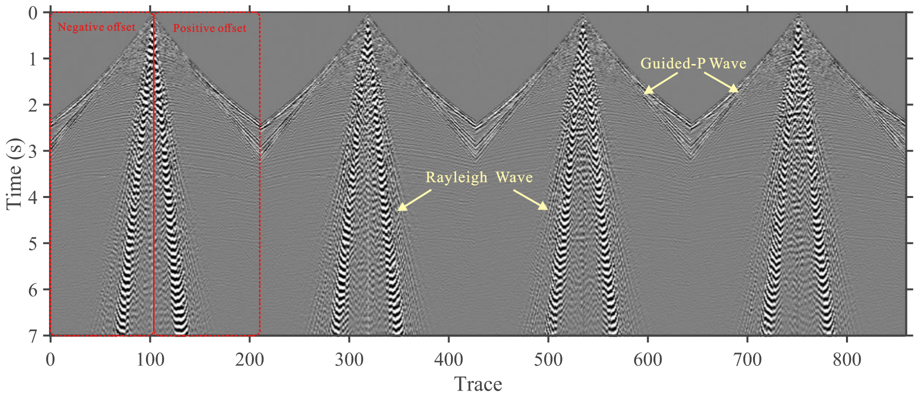

Fig. 15 The field shot gathers acquired for oil and gas exploration include obvious Rayleigh and guided-P waves. The red frames indicate the seismic traces of negative and positive offsets used for dispersion imaging

and positive offsets of the shot gathers in Fig. 15. The guided-P and Rayleigh wave dispersion energy can be clearly identified. Compared with Rayleigh wave, the strong dispersion energy of guided-P wave is distributed in a higher velocity range and has a wider frequency band.

In Fig. 17a, the dispersion curves of two Rayleigh wave modes and three guided-P wave modes are extracted from the dispersion image in Fig. 16a, as the gray dotted lines demonstrated. The initial velocity model for inversion is set as the uniform layers of thickness 20 m with increasing velocity. According to the integrated inversion, the v_S and v_P models are obtained and denoted by the red lines in Fig. 17e. Regardless of Rayleigh or guided-P waves, the inverted dispersion curves are in good agreement with the observed data, as shown in Fig. 17a. In Fig. 17b, the complete dispersion curves including normal and leaking modes are calculated using the inversion results. From the Jacobian matrix in Fig. 17c, it can be found that higher-mode guided-P wave are more sensitive to the v_P of deeper layers than the fundamental mode. In Fig. 17d, the sensitivity values of the v_S and v_P are calculated by adding the summing the absolute values of the sensitivities of each layer in the v_S and v_P regions of the Jacobian matrix. Since the dispersion information of the guided-P wave has one more mode than the surface wave, there is a high sensitivity value to the v_P in the deep layers.

Figure 18a and b shows the all 70 sets of picked dispersion curves corresponding to the positive and negative offsets. The inverted dispersion curves are shown in Fig. 18c and d. The inversion results are demonstrated by the red and blue lines in Fig. 18e and f. Based on the 1D approximation of surface wave analysis method, the inverted 1D velocity structures reflect the subsurface structures below the linear receiver lines (Mi et al. 2020). Hence, the inverted 1D v_S and v_P structures are located at the midpoints of the according receiver spreads. The velocity structures at other coordinates are obtained by weighted average of the two nearest 1D velocity structures (v_1 and v_2), and the distances are x_1 and x_2. Then the unknown 1D velocity structure v_0 is interpolated as: $v_0=\frac{v_1x_2}{x_1+x_2}+\frac{v_2x_1}{x_1+x_2}$. In Fig. 19, the pseudo-2D v_S and v_P profiles are constructed by the inverse distance weighting interpolation method. The Poisson's ratio profile is converted from the v_S and v_P profiles, which is helpful for the characterization of near-surface sediments, assessing the lithology of subsurface and geotechnical investigations (Ivanov et al. 2006).

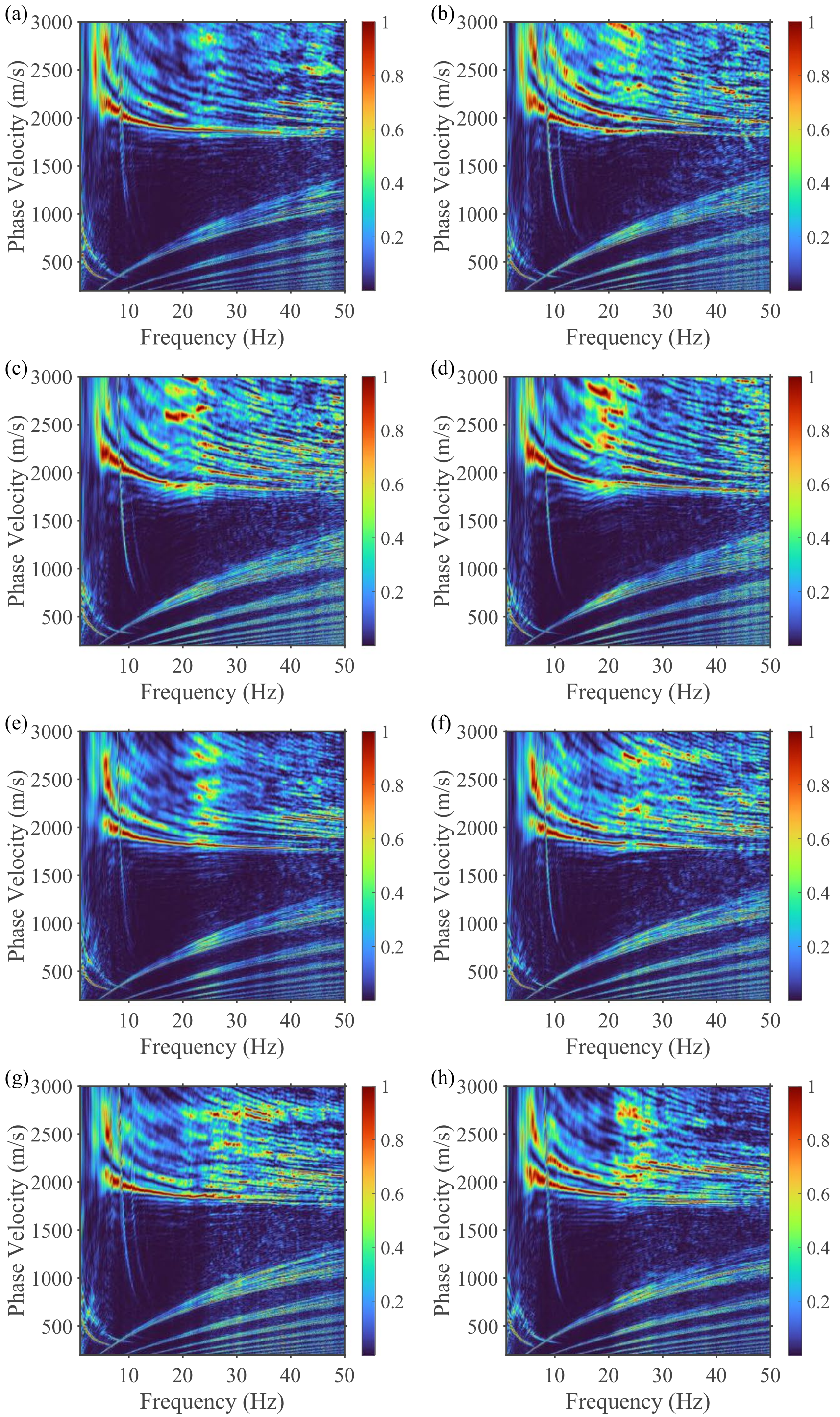

Fig. 16 (**a–d**) The dispersion images obtained from the negative offsets of the shot gathers in Fig. 15; (**e–h**) The dispersion images obtained from the positive offsets of the shot gathers in Fig. 15

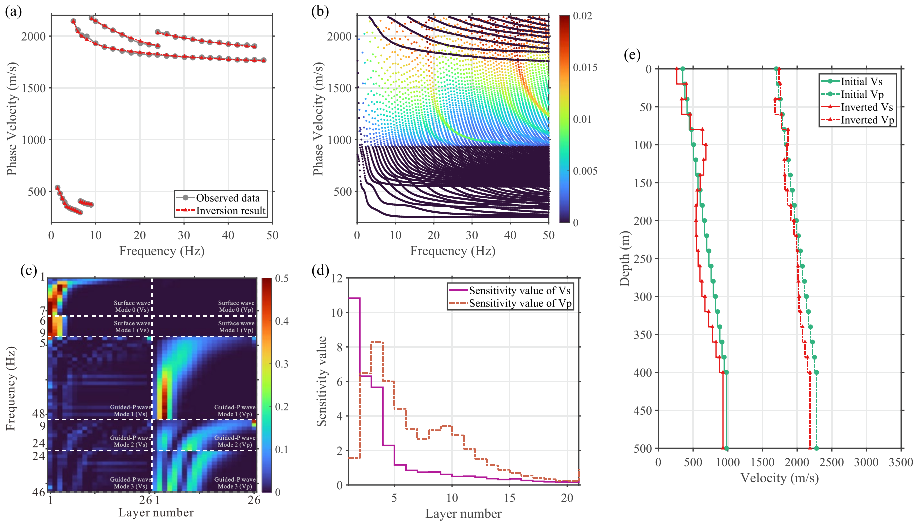

Fig. 17 (**a**) The fitting of the integrated inversion result with the observed surface and guided-P wave dispersion data; (**b**) The complete dispersion curves including normal and leaking modes calculated using the integrated inversion results; (**c**) The Jacobian matrixes of the integrated inversion method; (**d**) The sensitivity values of the v_S and v_P; (**d**) The v_S and v_P inversion results of the integrated inversion method

There are three formations distinguished by the black dashed lines in Fig. 19. For the v_S and Poisson's ratio profiles, the velocity interfaces are located at the depth around 100 and 250 m. However, the first velocity interface of v_P profile differs from v_S and locates at the depth around 150 m. This is caused by the influence of water content. Groundwater is defined as the water from rainwater or melting ice that soaks into the soil and is stored in the rock pores. In the unsaturated zone, the rock pores contain both air and water while the rock pores in the saturated zone are completely filled with water (Wang et al. 2021a, b). Theoretically, v_S and v_P are related to the mechanical parameters of rock. The compressibility of the pore fluid has a greater impact on v_P compared with the soil skeleton. The pore fluid dominates the v_P of the saturated media. Since the pore fluid has no shearing resistance, v_S can depict the variability of the solid matrix regardless the presence of fluid (Foti et al. 2014). In Fig. 20, combining the integrated inversion results and the available geological information, the near-surface geological model is constructed. The formation lithology from shallow to deep is silty clay, conglomerate and marlstone. The distribution of groundwater ranges in depth from about 50–150 m.

We also apply conventional individual inversion of surface wave dispersion curves to the 2D survey line, and the v_S result is shown in Fig. 21. Compared with the integrated inversion result, the results of the two methods are basically consistent, with only slight differences at the bedrock interface at a few coordinate positions. The first-arrival traveltime tomography method is also a commonly used means to characterize the shallow velocity structures. Here, first-arrival traveltime tomography is used to construct the 2D v_P profile to validate the integrated inversion results. Figure 22a is the picked first-arrival travel time for tomography inversion, and the red dashed frame represents the region of the pseudo-2D profile of the integrated inversion. Figure 22b is the inversion result of first-arrival traveltime tomography. The v_P model obtained by first-arrival traveltime tomography can detect the subsurface structure with a maximum depth of 1500 m, which is larger than surface

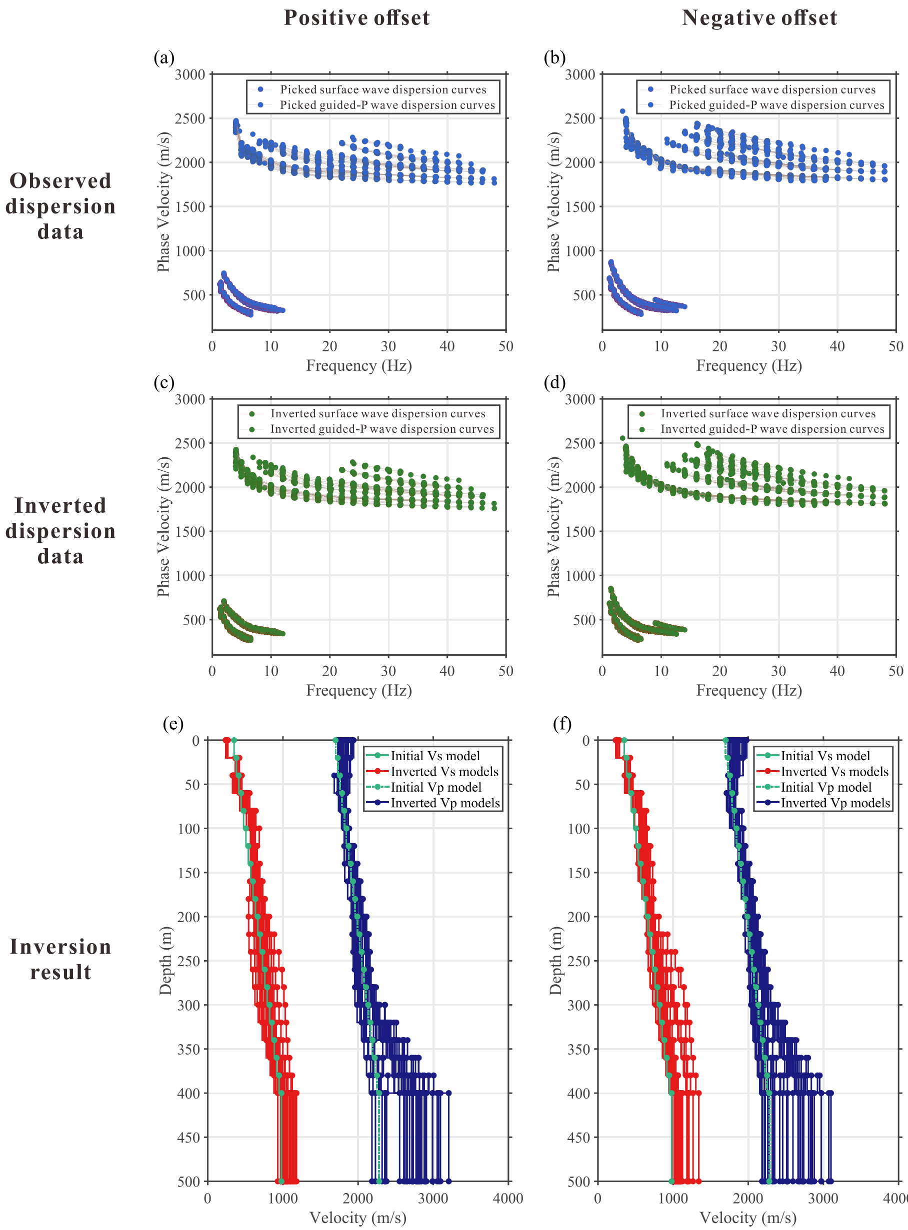

Fig. 18 (**a**) and (**b**) The all 70 sets picked dispersion curves of the positive and negative offsets; (**c**) and (**d**) The inverted dispersion curves of the positive and negative offsets; (**e**) and (**f**) The integrated inversion results of the positive and negative offsets

and guided-P waves. For the convenience of comparison, we show the part of first-arrival traveltime tomography result above the depth of 400 m and the part of the same coordinate range of the integrated inversion v_P result in Fig. 23a and b. Because the acquisition geometry and parameters were designed for reflection wave seismic exploration, the receiver

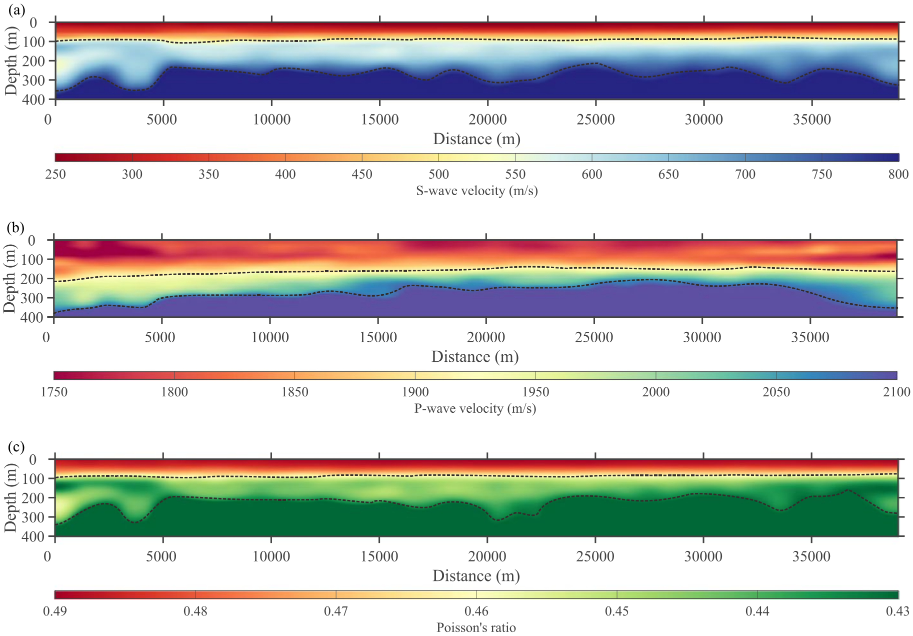

Fig. 19 (**a**) and (**b**) The pseudo-2D v_S and v_P profiles constructed by interpolating the 1D inversion results; (**c**) The 2D Poisson's ratio profile converted from the v_S and v_P profiles in (**a**) and (**b**)

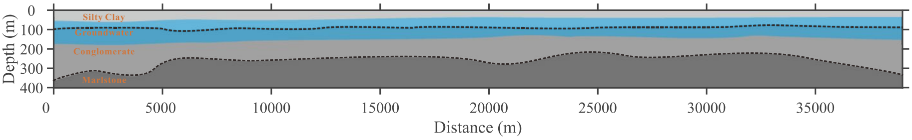

Fig. 20 The geological model interpreted from the integrated inversion results and the available geological information

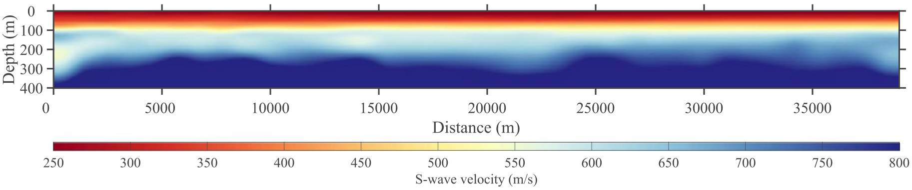

Fig. 21 The pseudo-2D v_S obtained by the conventional individual inversion of surface wave dispersion curves

interval is large, resulting in insufficient resolution of first-arrival traveltime tomography for shallow velocity structures. In Fig. 23, the 1D v_S and v_P models are extracted from the 2D structures obtained by the integrated inversion, conventional individual inversion and first-arrival traveltime tomography at the locations of B1 and B2, which are indicated by the gray arrows in Fig. 24. In contrast, the overall velocity trends of the results are basically

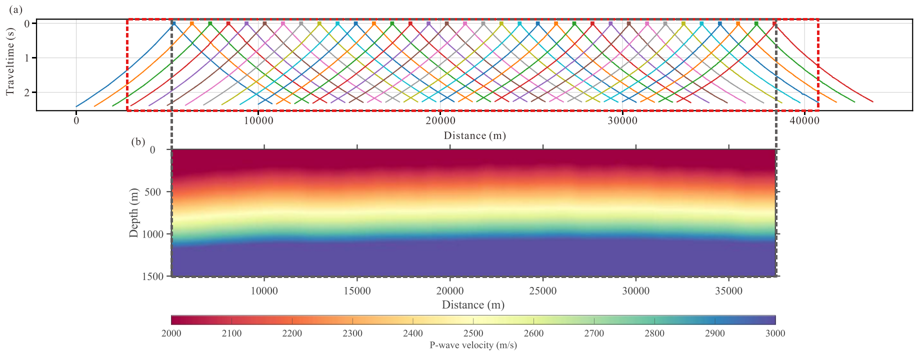

Fig. 22 (**a**) The picked first-arrival traveltime for tomography inversion; (**b**) The 2D v_P profile obtained by first-arrival traveltime tomography

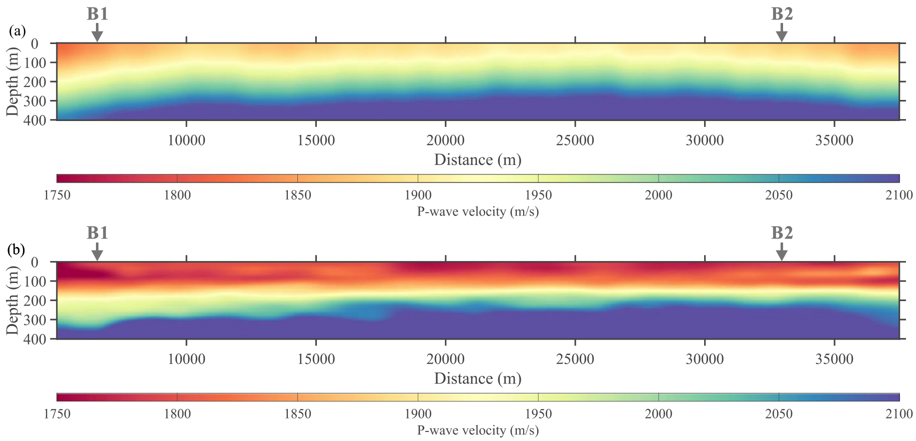

Fig. 23 (**a**) The 2D v_P profile above depth 400 m obtained from first-arrival traveltime tomography; (**b**) The part 2D v_P profile of the integrated inversion with the same coordinate range of first-arrival traveltime tomography result

the same, however, the integrated inversion method can characterize more details and its results are in better agreement with the borehole data. This further proves the practicability and reliability of the proposed integrated inversion method.

5 Discussion

Since the guided-P wave dispersion curves are determined by complex-valued leaking modal solutions, it requires higher computational cost compared to the calculation of surface-wave dispersion curves (Kennett 2023). Therefore, an accurate and efficient calculation method of guided-P wave dispersion curves is crucial for the inversion and application.

In addition, the correct identification of different mode dispersion curve is usually a prerequisite for the subsequent inversion. For geological conditions with low Poisson's ratio, the ranges of v_P and v_S may overlap. This will cause the surface and guided-P wave

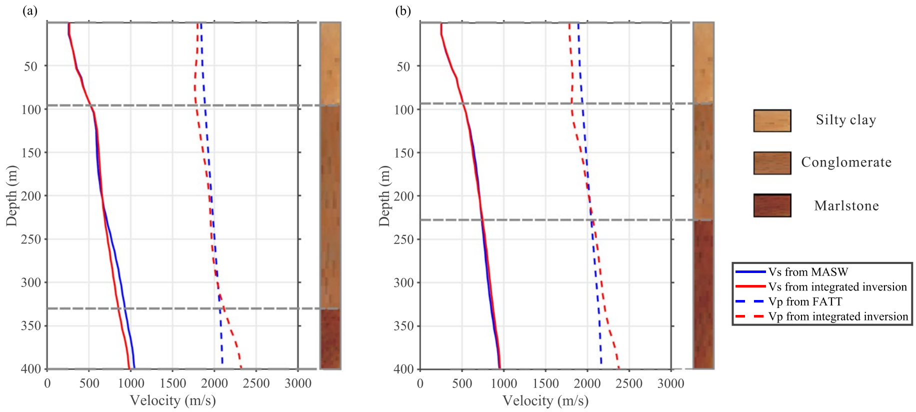

Fig. 24 (**a**) and (**b**) The comparison of conventional individual inversion, first-arrival traveltime tomography and integrated inversion results at the location of B1 and B2

dispersion curves to intermingle and couple together. On the other hand, for velocity models containing high- or low-velocity interlayers, the energy of guided-P wave in the dispersion images may become discontinuous and fragmented, and its attenuation coefficients are irregular (Boiero et al. 2013). These situations pose challenges to accurately extract and correctly identify the dispersion curves of different modes. To avoid this problem, the new misfit function based on the secular function, full-waveform inversion and dispersion spectrum inversion have the unique advantages (Maraschini et al. 2010; Dou and Ajo-Franklin 2014; Dal Moro et al. 2018).

Furthermore, leaky surface wave is another category of leaking mode that is obviously different from guided-P wave. Due to the severe attenuation of leaky surface wave, its dispersion curves are more difficult to extract in the field seismic data (Gao et al. 2014). However, its contribution and impact on the dispersion curve inversion should not be ignored. Therefore, it deserves further analysis and research in the future.

6 Conclusions

Compared with the surface waves corresponding to the normal modes, which are widely studied and applied, there is less research on the guided P waves corresponding to the leaking modes. Guided-P waves carry the dispersion information that can be used to construct the subsurface v_P structures. We presented an integrated inversion method of guided-P and surface wave dispersion curves to simultaneously estimate v_P and v_S models in this paper. Through the calculation of Jacobian matrix, the sensitivity of dispersion curves is quantitatively analyzed. It is proved that the dispersion curves of guided-P and surface waves are, respectively, sensitive to the v_P and v_S. Synthetic model tests demonstrate the proposed integrated inversion method can accurately estimate the v_P and v_S models, and effectively identify low-velocity interlayers. The integrated inversion method is also applied to the field seismic data acquired for oil and gas prospecting. The pseudo-2D v_P, v_S and Poisson's ratio inversion results are of significance for near-surface geological interpretation. The comparison with the first-arrival traveltime tomography result further demonstrates the accuracy and practicality of the proposed integrated inversion method.

Not only in the field of exploration seismic, the guided-P wave dispersion information can be extracted from the earthquake seismic, engineering seismic and ambient noise. The proposed inversion method can exploit previously neglected guided P waves to characterize the subsurface v_P structures. This compensates for the inherent defect that the surface-wave dispersion curve is mainly sensitive to the v_S structures and shows broad and promising application prospects.

Acknowledgements This work was supported by the National Natural Science Foundation of China (Grant No. 42174140).

Author's Contribution ZW contributed to methodology, software, formal analysis, and writing—original draft. CS contributed to conceptualization and data curation. DW contributed to visualization and investigation.

Data Availability The datasets used in this paper are available (https://github.com/GEOWZN/IIGS).

Declarations

Conflict of interest We declare: "No conflict of interest exists in the submission of this manuscript, and manuscript is approved by all authors for publication. We would like to declare on behalf of my co-authors that the work described was original research that has not been published previously, and not under consideration for publication elsewhere, in whole or in part. All the authors listed have approved the manuscript that is enclosed."

References

Aki K, Richards PG (1980) Quantitative seismology. W. H. Freemen and Company
Bohlen T, Fernandez MR, Ernesti J, Rheinbay C, Rieder A, Wieners C (2021) Visco-acoustic full waveform inversion: from a DG forward solver to a Newton-CG inverse solver. Comput Math Appl 100:126–140
Boiero D, Socco LV (2014) Joint inversion of Rayleigh-wave dispersion and P-wave refraction data for laterally varying layered models. Geophysics 79(4):1JA-Z105
Boiero D, Wiarda W, Vermeer P (2013) Surface- and guided-wave inversion for near-surface modeling in land and shallow marine seismic data. Lead Edge 32:638–646
Buchen PW, Ben-Hador R (1996) Free-mode surface-wave computations. Geophys J Int 124(3):869–887
Burg KE, Ewing M, Press F, Stulken EJ (1951) A seismic wave guide phenomenon. Geophysics 16(4):594–612
Cardarelli E, Fischanger F (2006) 2D data modelling by electrical resistivity tomography for complex subsurface geology. Geophys Prospect 54(2):121–133
Cercato M (2007) Computation of partial derivatives of Rayleigh-wave phase velocity using second-order subdeterminants. Geophys J Int 170(1):217–238
Chen X (1993) A systematic and efficient method of computing normal modes for multilayered half-space. Geophys J Int 115(2):391–409
Cochran MD, Woeber AF, De Bremaecker JC (1970) Body waves as normal and leaking modes, 3. Pseudo modes and partial derivatives on the (+−) sheet. Rev Geophys 8(2):321–357
Constable SC, Parker RL, Constable CG (1987) Occam's inversion: a practical algorithm for generating smooth models from electromagnetic sounding data. Geophysics 52(3):289–300
Cox M, Scherrer EF, Chen R (1999) Static corrections for seismic reflection surveys. Society of Exploration Geophysicists
Dai T, Xia J, Ning L, Xi C, Liu Y, Xing H (2021) Deep learning for extracting dispersion curves. Surv Geophys 42:69–95
Dal Moro G (2020) The magnifying effect of a thin shallow stiff layer on Love waves as revealed by multicomponent analysis of surface waves. Sci Rep 10(1):9071
Dal Moro G, Pipan M (2007) Joint inversion of surface wave dispersion curves and reflection travel times via multi-objective evolutionary algorithms. J Appl Geophys 61:56–81

Dal Moro G, Moustafa SSR, Al-Arifi NS (2018) Improved holistic analysis of rayleigh waves for single- and multi-offset data: joint inversion of rayleigh-wave particle motion and vertical- and radial-component velocity spectra. Pure Appl Geophys 175:67–88

Dorman J, Ewing M (1962) Numerical inversion of seismic surface wave dispersion data and crust – mantle structure in the New York – Pennsylvania area. J Geophys Res 67(13):5227–5241

Dou S, Ajo-Franklin JB (2014) Full-wavefield inversion of surface waves for mapping embedded low-velocity zones in permafrost. Geophysics 79(6):EN107–EN124

Dunkin JW (1965) Computation of modal solutions in layered, elastic media at high frequencies. Bull Seismol Soc Am 55(2):335–358

Fichtner A, Hofstede C, Kennett BLN, Nymand NF, Lauritzen ML, Zigone D, Eisen O (2023) Fiber-optic airplane seismology on the Northeast Greenland ice stream. The Seismic Record 3(2):125–133

Foti S, Parolai S, Albarello D, Picozzi M (2011) Application of surface-wave methods for seismic site characterization. Surv Geophys 32(6):777–825

Foti S, Lai CG, Rix GJ, Strobbia C (2014) Surface wave methods for near-surface site characterization. CRC Press, Boca Raton

Foti S, Hollender F, Garofalo F, Albarello D, Asten M, Bard PY, Comina C, Cornou C, Cox B, Giulio GD, Forbriger T, Hayashi K, Lunedei E, Martin A, Mercerat D, Ohrnberger M, Poggi V, Renalier F, Sicilia D, Socco LV (2018) Guidelines for the good practice of surface wave analysis: a product of the Inter PACIFIC project. Bull Earthq Eng 16:2367–2420

Gao L, Xia J, Pan Y (2014) Misidentification caused by leaky surface wave in high-frequency surface wave method. Geophys J Int 199(3):1452–1462

Ghanem KG, Sharafeldin SM, Saleh AA, Mabrouk WM (2017) A comparative study of near-surface velocity model building derived by 3D traveltime tomography and dispersion curves inversion techniques. J Petrol Sci Eng 154:126–138

Gilbert F (1964) Propagation of transient leaking modes in a stratified elastic waveguide. Rev Geophys 2(1):123–153

Gilbert F, Backus GE (1966) Propagator matrices in elastic wave and vibration problems. Geophysics 31(2):326–332

Goldstone L, Oliner AA (1959) Leaky-wave antennas I: rectangular waveguides. IRE Trans Antennas Propag 7(4):307–319

Haddon RAW (1984) Computation of synthetic seismograms in layered earth models using leaking modes. Bull Seismol Soc Am 74(4):1225–1248

Hakoda C, Lissenden CJ (2018) Using the partial wave method for wave structure calculation and the conceptual interpretation of elastodynamic guided waves. Appl Sci 8(6):966

Haskell NA (1953) The dispersion of surface waves on multilayered media. Bull Seismol Soc Am 43(1):17–34

Ivanov J, Miller RD, Xia J, Steeples D, Park CB (2006) Joint analysis of refractions with surface waves: an inverse solution to the refraction-traveltime problem. Geophysics 71(6):R131–R138

Jackson DR, Baccarelli P, Burghignoli P, Fuscaldo W, Galli A, Lovat G (2019) A history of leaky waves and leaky-wave antennas. In: 2019 Ursi International Symposium on Electromagnetic Theory (EMTS). IEEE, pp 1–4

Kennett BLN (2023) Interacting seismic waveguides: multimode surface waves and leaking modes. Seismica. https://doi.org/10.26443/seismica.v2i1.282

Kennett BLN, Clarke TJ (1983) Rapid calculation of surface wave dispersion. Geophys J Int 72(3):619–631

Knopoff L (1964) A matrix method for elastic wave problems. Bull Seismol Soc Am 54(1):431–438

Li J, Hanafy S, Schuster G (2018) Wave-equation dispersion inversion of guided P waves in a waveguide of arbitrary geometry. J Geophys Res: Solid Earth 123(9):7760–7774

Li Z, Shi C, Chen X (2021) Constraints on crustal P wave structure with leaking mode dispersion curves. Geophys Res Lett 48(20):e2020GL091782

Li Z, Shi C, Ren H, Chen X (2022) Multiple leaking mode dispersion observations and applications from ambient noise cross-correlation in Oklahoma. Geophys Res Lett 49(1):e2021GL096032

Lowe MJS (1995) Matrix techniques for modeling ultrasonic waves in multilayered media. IEEE Trans Ultrason Ferroelectr Freq Control 42(4):525–542

Maraschini M, Ernst F, Foti S, Socco LV (2010) A new misfit function for multimodal inversion of surface waves. Geophysics 75(4):G31–G43

Mari JL (1984) Estimation of static corrections for shear-wave profiling using the dispersion properties of Love waves. Geophysics 49(8):1169–1179

Mazzotti M, Bartoli I, Marzani A, Viola E (2013) A coupled SAFE-2.5 D BEM approach for the dispersion analysis of damped leaky guided waves in embedded waveguides of arbitrary cross-section. Ultrasonics 53(7):1227–1241

McMechan GA, Yedlin MJ (1981) Analysis of dispersive waves by wavefield transformation. Geophysics 46:869–874
Menke W (2012) Geophysical data analysis: discrete inverse theory: MATLAB edition. Academic press
Mi B, Xia J, Bradford JH, Shen C (2020) Estimating Near-surface shear-wave-velocity structures via multichannel analysis of Rayleigh and love waves: an experiment at the boise hydrogeophysical research site. Surv Geophys 41:323–341
Miller RD, Xia J, Park CB, Ivanov JM (1999) Multichannel analysis of surface waves to map bedrock. Lead Edge 18(12):1392–1396
Monticone F, Alu A (2015) Leaky-wave theory, techniques, and applications: from microwaves to visible frequencies. Proc IEEE 103(5):793–821
Oliver J (1964) Propagation of PL waves across the United States. Bull Seismol Soc Am 54(1):151–160
Oliver J, Major M (1960) Leaking modes and the PL phase. Bull Seismol Soc Am 50(2):165–180
Pan Y, Gao L, Bohlen T (2019) High-resolution characterization of near-surface structures by surface-wave inversions: from dispersion curve to full waveform. Surv Geophys 40:167–195
Park CB, Miller RD, Xia J (1999) Multichannel analysis of surface waves. Geophysics 64(3):800–808
Phinney RA (1961) Leaking modes in the crustal waveguide: 1. The oceanic PL wave. J Geophys Res 66(5):1445–1469
Pilant WL (1972) Complex roots of the Stoneley-wave equation. Bull Seismol Soc Am 62(1):285–299
Radovich BJ, De Bremaecker JC (1974) Body waves as normal and leaking modes—leaking modes of Love waves. Bull Seismol Soc Am 64(2):301–306
Rayleigh JWS (1885) On waves propagated along the plane surface of an elastic solid. Proc Lond Math Soc 17:4–11
Robertsson JOA, Holliger K, Green AG, Pugin R, De Iaco R (1996) Effects of near-surface waveguides on shallow high-resolutin seismic refraction and reflection data. Geophys Res Lett 23(5):495–498
Rosenbaum JH (1960) The long-time response of a layered elastic medium to explosive sound. J Geophys Res 65(5):1577–1613
Roth M, Holliger K (1999) Inversion of source-generated noise in high-resolution seismic data: observations and modeling. Geophys J Int 18:1402–1406
Ryden N, Lowe MJS (2004) Guided wave propagation in three-layer pavement structures. The J Acoust Soc Am 116(5):2902–2913
Sheriff RE, Geldart LP (1995) Exploration seismology. Cambridge University Press
Shtivelman V (2004) Estimating seismic velocities below the sea-bed using surface waves. Near Surf Geophys 2(4):241–247
Smith RE, Houde-Walter SN, Forbes GW (1991) Numerical determination of planar waveguide modes using the analyticity of the dispersion relation. Opt Lett 16(17):1316–1318
Socco LV, Strobbia C (2004) Surface-wave method for near-surface characterization: a tutorial. Near Surf Geophys 2:165–185
Socco LV, Foti S, Boiero D (2010) Surface wave analysis for building near-surface velocity models – established approaches and new perspectives. Geophysics 75(5):75A83-75A102
Somville O (1930) A propos d'une onde longue dans la premiére phase de quelques séismogrammes. Gerlands Beitr Geophys 27:437–442
Su SS, Dorman J (1965) The use of leaking modes in seismogram interpretation and in studies of crust-mantle structure. Bull Seismol Soc Am 55(6):989–1021
Sun C, Wang Z, Wu D, Cai R, Wu H (2021) A unified description of surface waves and guided waves with relative amplitude dispersion maps. Geophys J Int 227(3):1480–1495
Thomson WT (1950) Transmission of elastic waves through a stratified solid medium. J Appl Phys 21(2):89–93
Tikhonov AN, Arsenin VY (1977) Solution of ill-posed problems. VH Winston ans Sons, Washington DC
Virieux J (1986) P-SV wave propagation in heterogeneous media: velocity-stress finite-difference method. Geophysics 51(4):889–901
Vozoff K, Jupp DLB (1975) Joint inversion of geophysical data. Geophys J Int 42:977–991
Wang CY, Herrmann RB (1980) A numerical study of P-, SV-, and SH-wave generation in a plane layered medium. Bull Seismol Soc Am 70(4):1015–1036
Wang W, Chen P, Dueker K, Zhang Y, Lee E, Mu D, Keifer I, Jiao J (2021a) Coevolution of weathering front and water table. Geophys Res Lett 48(20):e2021GL092916
Wang Z, Sun C, Wu D (2021b) Automatic picking of multi-mode surface-wave dispersion curves based on machine learning clustering methods. Comput Geosci 153:104809
Wang Z, Sun C, Wu D (2023) Near-surface Site characterization based on joint iterative analysis of first-arrival and surface-wave data. Surv Geophys 44:357–386

Watson TH (1972) A real frequency, complex wave-number analysis of leaking modes. Bull Seismol Soc Am 62(1):369–384
Wu B, Chen X (2017) Accurate computation of leaky modes for anomalous layered models. Ann Geophys 60(6):S0663–S0663
Wu D, Wang X, Su Q, Zhang T (2019) A MATLAB package for calculating partial derivatives of surface-wave dispersion curves by a reduced delta matrix method. Appl Sci 9(23):5214
Xia J, Miller RD, Park CB (1999) Estimation of near-surface shear-wave velocity by inversion of Rayleigh waves. Geophysics 64:691–700
Yang J, Huang J, Zhu H, McMechan G, Li Z (2022) Introduction to a two-way beam wave method and its applications in seismic imaging. J Geophys Res: Solid Earth 127:e2021JB023357
Zhang J, Toksoz MN (1998) Nonlinear refraction traveltime tomography. Geophysics 63(5):1726–1737
Znak P, Kashtan B, Bakulin A (2015) Guided waves and rayleigh leaking modes with outpost algorithm. In: 77th Annual International Conference and Exhibition, EAGE, Extended Abstracts, pp 1–5